Gallium Oxide Thin Films for Optoelectronic Applications

by

Sundar Babu Isukapati

Submitted in Partial Fulfillment of the Requirements

for the Degree of

Master of Science

in the

Electrical Engineering

Program

YOUNGSTOWN STATE UNIVERSITY

May 2018

Gallium Oxide Thin Films for Optoelectronic Applications

Sundar Babu Isukapati

I hereby release this thesis to the public. I understand that this thesis will be made available from the OhioLINK ETD Center and the Maag Library Circulation Desk for public access. I also authorize the University or other individuals to make copies of this thesis as needed for scholarly research.

Signature:

Sundar Babu Isukapati, Student Date

Approvals:

Dr. Tom Nelson Oder, Thesis Advisor Date

Dr. Faramarz Mossayebi, Committee Member Date

Dr. Eric MacDonald, Committee Member Date

Dr. Salvatore A. Sanders, Dean of Graduate Studies Date

ABSTRACT

Gallium oxide (Ga_2O_3) belongs to the family of transparent conducting oxides (TCOs) which have emerged as attractive semiconductor material due their excellent properties. TCOs offer the combination of high conductivity along with excellent transparency in the visible region and a large direct band gap of 4.9 eV. These open the scope for applications for deep UV optical and high power/high voltage electronic device applications.

The objective of this research was to fabricate high quality Ga_2O_3 thin films by magnetron sputtering which would be used to fabricate optoelectronic devices. The thin films were deposited on double polished c-plane sapphire substrates. Four investigations were conducted in order to optimize the quality of the thin films. First, the effect of using different Ar/O_2 mixture for deposition was investigated. Second, the post deposition annealing was investigated where the films were annealed in vacuum and in different gas environments. Third, the effect of different substrate temperature from 20 ^{o}C to 800 ^{o}C was investigated. The fourth investigation was where different amounts of tin were introduced in order to perform n-type doping of the films. The structural and elemental compositional properties of the films were determined using x-ray diffraction and energy dispersive spectrometry measurements. ($\bar{2}\,0\,1$) oriented β-Ga_2O_3 single crystal thin films were obtained when deposited using 100 % Ar at 500 ^{o}C. The optical characteristics obtained by UV-VIS spectroscopy measurements showed excellent transmission of 90 - 95% and optical bandgaps of 4.7- 5.0 eV. Addition of tin dopants in the films produced a decrease in the optical bandgaps with increasing concentration of tin to the films.

Acknowledgement

Before anything else, it is a great pleasure to acknowledge and express my deepest thanks and gratitude to my advisor Dr. Tom Nelson Oder for his continuous support, motivation, enthusiasm, and immense knowledge over the years in this research. Without his guidance and persistent help, this thesis would not have been possible.

I would like to thank my thesis committee: Dr. Faramarz Mossayebi and Dr. Eric MacDonald for their support and guidance. I would also like to thank Dr. Jalal Jalali, *Chair and Professor of Electrical Engineering* and Youngstown state University for giving me an opportunity to work in the Department of Physics & Astronomy as a graduate research assistant.

Assistances by Ray Hoff (for XRD measurements) from Department of Chemistry and Matt Caputo (for EDS measurements) from the Materials Science and Engineering program are also gratefully acknowledged.

Finally, I would like to extend my deepest gratitude to my parents for their love and encouragement. My sincere thanks also go to all the colleagues and people who helped me out with their abilities.

Contents

ABSTRACT iii

Acknowledgement iv

List of Figures ix

List of tables xi

Chapter 1 1

Gallium Oxide and Different Growth techniques 1

1.1 Introduction 1

1.2 Physical Properties 2

1.2.1 Polymorphs of Ga_2O_3 2

1.2.2 Crystal Structure 3

1.2.3 Thermal Properties 3

1.2.4 Optical Properties 4

1.2.5 Electronic properties 5

1.3 Why Ga_2O_3? 6

1.4 Bulk Growth 7

1.4.1 Floating-zone method (FZ) 7

1.4.2 Czochralski method (CZ) 8

1.4.3 Edge defined film fed growth (EFG) 8

1.5 Wafer Production 9

1.6 Epitaxial Thin Film Growth ... 10
1.6.1 Molecular Beam Epitaxy (MBE) ... 11
1.6.2 Metalorganic Chemical Vapor Deposition (MOCVD) ... 12
1.6.3 Halide vapor phase epitaxy (HVPE) ... 12
1.6.4 Mist-CVD ... 13
Chapter 2 ... 15
Experimental Techniques ... 15
2.1 Physical Vapor Deposition ... 15
2.2 Sputter Deposition ... 17
2.2.1 Magnetron Sputtering ... 17
2.3 Rapid Thermal Processing ... 18
2.4 Energy dispersive X-ray spectroscopy (EDS or EDX) using Scanning Electron Microscopy (SEM) ... 19
2.5 X-ray Diffraction ... 22
2.6 Four-point probe Resistivity Measurements ... 24
2.7 UV-Vis Spectroscopy ... 25
Chapter 3 ... 27
The Growth of Gallium Oxide Thin Films Using Magnetron Sputtering ... 27
3.1 Vacuum System ... 28
3.2 Substrate holder and heater ... 29

3.3 Target and Gun assembly 29
3.4 Types of power supplies 31
3.4.1 Direct Current sputtering (DC) 31
3.4.2 Radio Frequency Sputtering (RF) 32
3.5 Temperature Controller and thermocouple 33
3.6 Vent Valve and Mass Flow controller 34
3.7 Substrate cleaning and thermal desorption 34
Chapter 4 36
Results and Analysis 36
4.1 Films deposited in gas mixtures of Argon (Ar) and Oxygen (O_2) 36
4.1.1 X-ray Diffraction (XRD) 37
4.1.2 Energy dispersive Spectroscopy (EDS) 38
4.1.3 UV-Vis Spectroscopy 39
4.1.4 Optical bandgap 40
4.2 Annealing treatment on single crystal gallium oxide thin films 42
4.2.1 X-ray Diffraction (XRD) 42
4.2.2 Resistivity measurements 44
4.2.3 Optical bandgap 45
4.3 Ga_2O_3 films deposited at various substrate temperatures in Ar/O_2 80/20 45
4.3.1 X-ray Diffraction 46

4.3.2 Energy dispersive Spectroscopy (EDS) 47

4.3.3 UV- Vis Spectroscopy 48

4.3.4 Optical Bandgap.. 49

4.4 Annealing in different gas atmospheres of 800 nm thick Gallium oxide film ... 50

4.4.1 X-ray Diffraction (XRD) 50

4.5 Doping Gallium oxide (Ga_2O_3) thin films with Tin (Sn) 52

4.5.1 EDS measurements 52

4.5.2 XRD measurements 54

4.5.3 Optical characteristics 55

4.5.4 Optical Bandgap.. 56

Chapter -5... 58

Conclusions and future work 58

5.1 Conclusion.. 58

5.2 Future work 59

References.. 60

List of Figures

Figure 1: Unit cell of Ga_2O_3, along c-axis (1), a-axis (2) and b-axis (3) [6] 3

Figure 2: Band structure of Ga_2O_3 [12]... 5

Figure 3: An EFG Furnace [18] 9

Figure 4: A 4-inch diameter β- Ga_2O_3 wafer [18]... 10

Figure 5: An MBE setup for Ga_2O_3 growth [28] 11

Figure 6: HVPE system for Ga_2O_3 growth [33]... 12

Figure 7: A Mist-CVD system for Ga_2O_3 growth [42] 14

Figure 8: (a) Vacuum evaporation (b, c) Sputter deposition (d, e) Ion plating (f) IBAD [47] 16

Figure 9: Magnetron sputtering mechanism [48].. 18

Figure 10: Rapid Thermal Processor 19

Figure 11: Schematic of SEM [50] 20

Figure 12: JOEL JSM-7600F.. 22

Figure 13: Bragg's law illustration [52].. 23

Figure 14: Bruker D8 Prospector close up.. 24

Figure 15: (a) Probe station (b) Schematic [54] (c) Keithley 2410 Source meter 25

Figure 16: UV-Vis Spectroscopy set up 26

Figure 17: Ocean optics USB 4000 spectrometer and light source 26

Figure 18: Sputter deposition chamber 27

Figure 19: Schematic of magnetron sputter sputtering deposition chamber [adapted from 55] 28

Figure 20: Sapphire substrate mounted on heater... 29

Figure 21: (a) Gallium oxide target (b) Tin target 30

Figure 22: Targets mounted on cathodes 31

Figure 23: DC power supply 32

Figure 24: RF power supply 33

Figure 25: Thermocouple read out 33

Figure 26: Mass flow controller 34

Figure 27: 3-inch c-plane sapphire substrate 35

Figure 28: XRD data of films deposited in various gases 37

Figure 29: EDS analysis on films deposited in (a) 100/0 O_2 (b) Ar/O_2 20/80 (c) Ar/O_2 50/50 (d) Ar/O_2 80/20 and (e) 100/0 Ar 38

Figure 30: Transmission results of films deposited in various gases 39

Figure 31: Absorbance results of films deposited in various gases 40

Figure 32: Tauc plot to determine optical bandgap 41

Figure 33: XRD data of single crystal thin Gallium oxide thin films annealed at various conditions 43

Figure 34: XRD data of films deposited at various temperatures 46

Figure 35: Films deposited in Ar/O_2 80/20 at various substrate temperatures (a) 20°C (b) 250°C (c) 500°C (d) 650°C and (e) 800°C 47

Figure 36: Transmission measurements on films deposited at various temperatures 48

Figure 37: Absorbance measurements on films deposited at various temperatures 49

Figure 38: XRD data of films annealed in various gases 51

Figure 40: XRD data of Ga_2O_3: Sn samples 54

Figure 41: Transmission measurements of uniformly doped samples 55

Figure 42: Absorbance measurements of uniformly doped samples 56

List of tables

Table 1: Ga_2O_3 vs other semiconductor material properties 7

Table 2: Optical bandgap of Ga_2O_3 deposited in various gases 42

Table 3: Optical bandgap of annealed single crystal thin films 45

Table 4: Optical bandgap of Ga_2O_3 deposited in various temperatures 49

Table 5: Optical bandgap of Ga_2O_3 : Sn 56

Chapter 1

Gallium Oxide and Different Growth techniques

1.1 Introduction

The electronics and the computing that we use today is due to the invention of silicon (Si) integrated circuit technology invented 50 years ago. But as all good things come to an end, it is time for silicon technology in semiconductor industry to end. In the year 1965, Gordon Moore stated that "the number of transistors in a dense integrated circuit doubles approximately every two years." [1] As of 2016, the largest number of transistors in a commercial single chip processor "Intel Broad well-EP Xenon" is 7.2 billion [2]. In silicon-based semiconductor industry, Moore's law can no longer be sustained. This is due to the limitations of the materials properties of silicon to handle the associate heat issues in packaging millions of transistors and leakage issues due to the shrinking technology.

In power electronics, it has been a constant challenge to create devices with great power density and energy efficiency. So, researchers have found silicon carbide (SiC) and gallium nitride (GaN), as an alternative to silicon in high temperature and power applications. Their high efficiency in power conversion has attracted the world of semiconductors. However SiC and GaN are not the only the semiconductor materials for next generation electronics. A new oxide compound semiconductor, gallium oxide (Ga_2O_3) which is promising because of its excellent properties and low cost [3].

Transparent conducting Oxides (TCO) have emerged as the latest semiconductor technology. TCO's opened the scope for research and wide range of applications. TCOs offer rare combination of conductivity along with transparency over the visible range. β –

phase of Ga_2O_3, with a large direct energy band gap of 4.8 eV to 4.9 eV and transmission of 90% over the visible region, opens the scope for deep UV optoelectronic as well as high temperature and voltage electronic device applications.

The aim of this research was to deposit high quality single crystal thin films on c-plane sapphire substrate using magnetron sputtering. To achieve conductive thin films, they would be doped with Sn. The final goal was to fabricate a UV-photodetector once the required high quality conductive thin films are obtained. Single crystal films were achieved, however, doping with Sn did not result in improvement of conductivity. Thus, the last objective of device fabrication was not realized.

1.2 Physical Properties

1.2.1 Polymorphs of Ga_2O_3

Ga_2O_3 forms different polymorphs namely α, β, γ, δ, ε [4]. Out of all the available forms β-form is the most popular polymorph of Ga_2O_3. β-Ga_2O_3 is the only stable polymorph out of all the forms over a wide temperature range till its melting point 1795°C. The remaining polymorphs are unstable and transform to the β form at temperatures above 750-900°C [5]. So, the thermal stability of β-Ga_2O_3 provides options to produce epitaxial layers and bulk single crystals.

1.2.2 Crystal Structure

β-Ga_2O_3 forms a base-centered monoclinic structure with lattice parameters a = 1.22 nm, b = 0.3 nm, c = 0.58 nm and β = 103.83° [6]. The unit cell structure of Ga_2O_3 is shown in Fig.1.

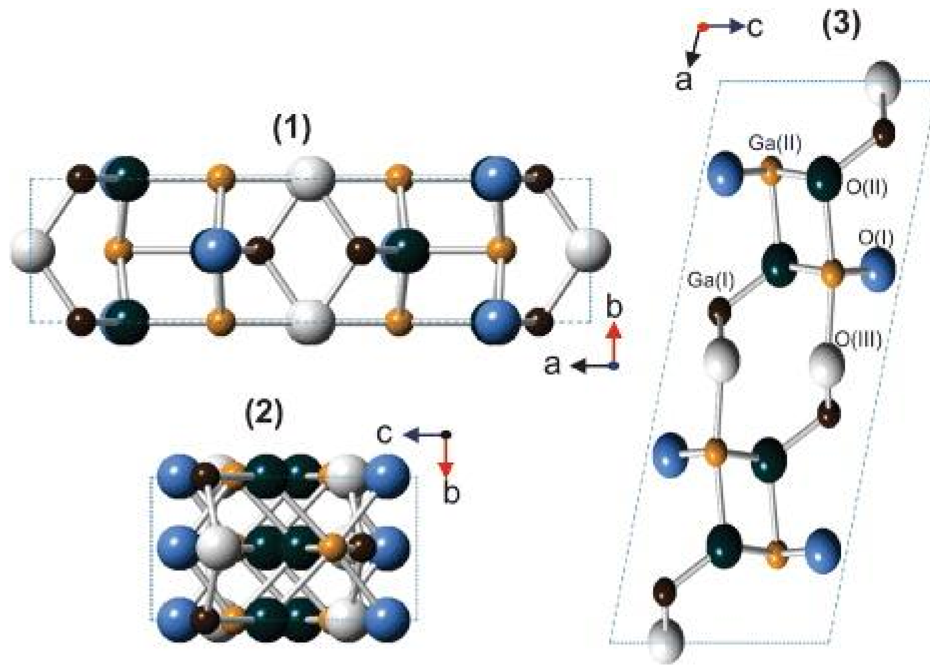

Figure 1: Unit cell of Ga_2O_3, along c-axis (1), a-axis (2) and b-axis (3) [6]

The subsets in Fig.1, show the unit cell of Ga_2O_3 along c, a and b-axis respectively. The unit cell of Ga_2O_3 has two inequivalent Ga sites Ga (I) and Ga (II) and three inequivalent O sites O (I), O (II) and O (III) as shown in Fig.1(3). Ga (I) has a tetrahedral geometry and Ga (II) forms an octahedral geometry [6].

1.2.3 Thermal Properties

Ga_2O_3 is the poor thermal conductor when compared with other semiconductors. When compared, its thermal conductivity is half that of Al_2O_3 which 23.2 W/mK. The

thermal conductivity is different along different directions due to crystalline anisotropy of Ga_2O_3. The thermal conductivity is large in [010] direction and smallest conductivity in [100] direction at all temperatures. The reported thermal conductivities in [100] direction is 13W/mK [7] and 21W/mK in [010] direction [8].

1.2.4 Optical Properties

β-Ga_2O_3 is colorless and extremely transparent till UV-C range which is till 280 nm of the light spectrum. Insulating β-Ga_2O_3 crystals are colorless or a yellowish color due to absorption in blue region and conductive β-Ga_2O_3 crystals have blue color which is due to increase in free carrier absorption in red and NIR regions [7, 8].

The absorption spectra might exhibit a cutoff absorption edge at 255 nm -260 nm with a shoulder around 270 nm. The absorption that happens at 255-260 nm is due to the transition of electrons from the valence band to conduction band [9].

The β-Ga_2O_3 can show three types of emissions such as UV (3.2 eV-3.6 eV), blue (2.8 eV-3.0 eV) and green (2.4 eV) bands [9-11]. With a band gap of 4.8 eV, UV band emission is independent of the growth technique and it is highly impossible that the UV band occurs because of band edge recombination but due to recombination of free electrons and self-trapped holes [11]. The blue band and resistivity in β-Ga_2O_3 crystals is correlated which show that oxygen vacancies contribute to the n-type conductivity of Ga_2O_3 crystals. The efficient green band emission occurs only after doping Ga_2O_3 with specific metals such as Sn, Si, Ge and to a small extent Cu, Fe and Li [11].

1.2.5 Electronic properties

Several studies have been conducted to study the band structure of Ga_2O_3 [12]. There are both direct and indirect band transitions in Ga_2O_3. Studies reveal that indirect transitions are weak when compared to the direct transitions [12]. The energy difference between direct and indirect transitions is relatively very small about 50 meV effectively making Ga_2O_3 a direct bandgap semiconductor. Fig.2 shows the band structure of Ga_2O_3.

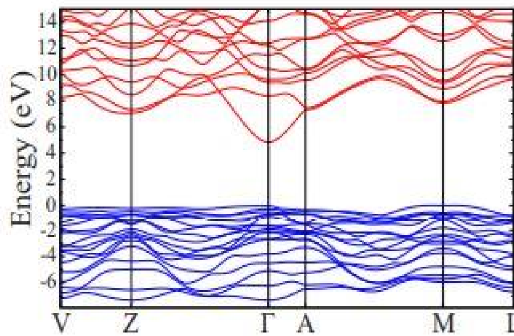

Figure 2: Band structure of Ga_2O_3 [12]

The band structure of Ga_2O_3 shows the energy gap between valence band and conduction band is approximately 4.9 eV. The valence band maximum (VBM) is almost flat due to which VBM is aligned with conduction band minimum (CBM) making it a direct band gap semiconductor. In a direct bandgap semiconductor, a direct recombination takes place with a release of energy equal to the bandgap. This feature of direct bandgap semiconductor is important for optical applications.

1.3 Why Ga_2O_3?

For power conversion, there are two important devices. One is switching transistors to control “on” and “off” states of current flow and the other is rectifying diodes to control the direction of current flow. In power devices there are two important losses. One is conduction which are due to resistive dissipation and the other switching losses due to capacitive components. So, the major benchmark for a power device is low on-resistance, low off-state leakage current, large break down voltage and fast switching recovery time.

The break down voltage of Ga_2O_3 is 8 MV/cm which is very large than SiC and GaN semiconductor materials which opens the scope for high voltage and high temperature applications [13].

The band gap of Ga_2O_3 reported is 4.9 eV which is much larger than SiC (3.3 eV) and GaN (3.4 eV) [13]. A large band gap enables strong electric field making it possible to use a thinner device for a given voltage. The thinner the device, the lower is the on-resistance and thus high efficiency.

The Baliga’s figure of merit (BFOM) which is criteria for rating semiconductor materials for power device applications shows that gallium oxide’s FOM is 10 times and 4 times larger than SiC and GaN respectively [13]. This is shown in Table 1.

Table 1: Ga_2O_3 vs other semiconductor material properties

	Si	SiC	GaN	β- Ga_2O_3
Bandgap (eV)	1.12	3.26	3.4	**4.9**
Dielectric constant ε	11.9	9.7	9.5	**10**
Electron mobility μ (cm^2/Vs)	1350	1000	900	**300(est.)**
Thermal conductivity (W/cmK)	1.5	4.9	2	**0.14**
Breakdown voltage E_b (MV/cm)	0.3	2.7	3.5	**8(est.)**
BFOM* ($\varepsilon \mu E_b^3$)	1	340	870	**3444**

1.4 Bulk Growth

Gallium oxide bulk crystals have been melded by various melt growth methods like floating-zone method (FZ) [14-18], Czochralski (CZ) method [19, 20], vertical Bridgman [21], and edge-defined film fed growth (EFG) methods [18, 22].

1.4.1 Floating-zone method (FZ)

Floating-zone is a relatively easy method and used to synthesize β-Ga_2O_3 single crystals. FZ technique is described clearly in [18]. Feed rods are prepared by a ceramic process in which Ga_2O_3 powder is ground and pressed into a rod shape. Generated rods

are then sediment by radiative heating. At a rate of 6 mm per hour Ga_2O_3 single crystals are grown [18].

1.4.2 Czochralski method (CZ)

CZ method for producing gallium oxide was first reported by Tomm [19]. A CZ apparatus with iridium crucible and an rf induction coil for heating are used [8]. In [20] researchers have reported that higher oxygen concentration is required for larger size bulk Ga_2O_3 to further scale up the crystal volume.

1.4.3 Edge defined film fed growth (EFG)

To produce large volumes of single crystal Ga_2O_3 wafers with large size, EFG is the most prominent growth method [18]. A schematic of the process is shown below in Fig. 3 [18]. Along with iridium die, a source powder was placed in an iridium crucible and heated by an rf induction coil at a growth atmosphere of a mixture of 98% nitrogen and 2% oxygen. For n-type doping SnO_2 or SiO_2 are added to the gallium oxide powder source. The capillary forces raise the melt through the split to the top surface as soon as the narrow split is dipped into the molten Ga_2O_3 in the crucible. Then a Ga_2O_3 single crystal bulk plate can be extracted from Ga_2O_3 seed crystal in contact with the molten Ga_2O_3 at the upper surface of the die. In this method, the growth is set along the [010] direction and ($\bar{2}$ 0 1) plane of Ga_2O_3 crystal with a growth rate of 15mm per hour [18].

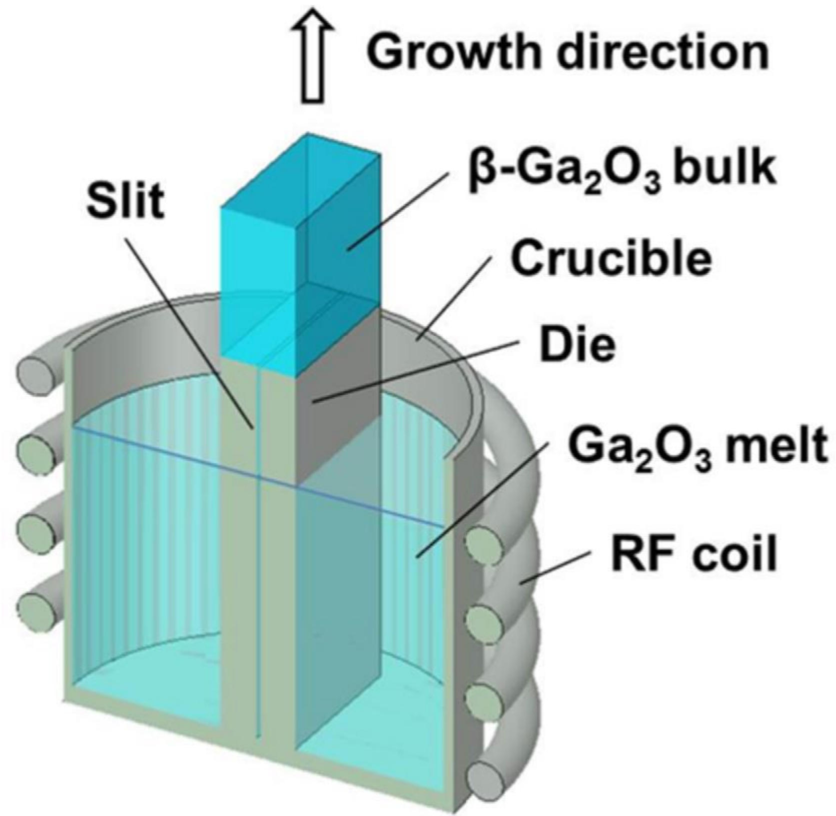

Figure 3: An EFG Furnace [18]

1.5 Wafer Production

Ga_2O_3 wafers are fabricated from EFG grown Ga_2O_3 bulk single crystals. EFG crystals are first annealed at 1450^oC in nitrogen gas to reduce stress and activate donor impurities in the crystal [18]. To achieve n-type doping conductivity, annealing at high temperatures is required for Sn-doped bulk crystals. After annealing, crystals are then cut into wafers by blade saw, grinder, wire saw and chemical mechanical polishing machine tools [18]. Fig. 4 shows a 4-inch diameter of a single crystal Ga_2O_3 wafer.

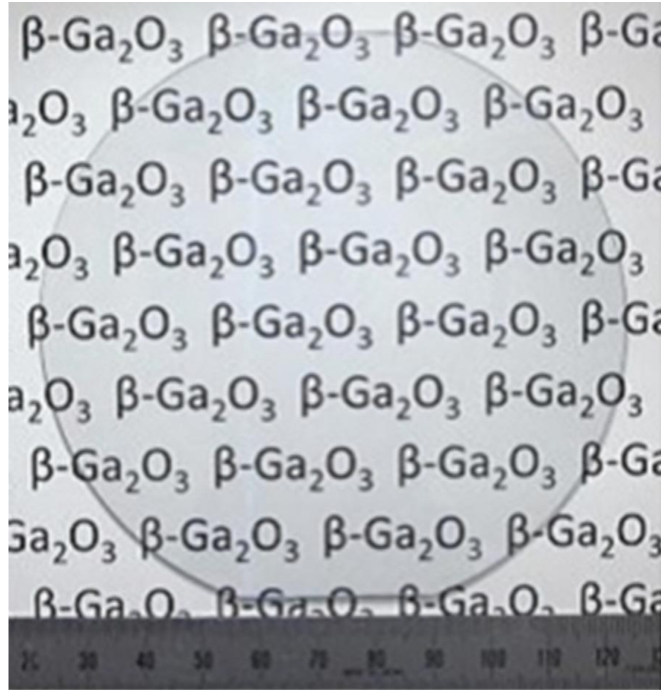

Figure 4: A 4-inch diameter β- Ga_2O_3 wafer [18]

1.6 Epitaxial Thin Film Growth

Poly and single crystal thin films are grown homoepitaxially on native gallium oxide substrate and heteroepitaxially on substrates like Al_2O_3, Si, GaAs, TiO_2, MgO etc. Some of the growth techniques are molecular beam epitaxy (MBE) [23-31], metalorganic chemical vapor deposition (MOCVD) [37-41], halide vapor phase epitaxy (HVPE) [32-36], mist chemical vapor deposition (mist-CVD) [42-46] and physical vapor deposition (PVD). Sputter deposition is part of the PVD method.

In this section, MBE, HVPE techniques are discussed followed by the introduction of mist-CVD and MOCVD techniques. PVD technique is used to grow thin films for this research, so it is explained in detail in Chapter 2.

1.6.1 Molecular Beam Epitaxy (MBE)

MBE is a popular growth technique to grow Ga_2O_3 thin films as it provides advantage to control growth parameters and doping concentration into epitaxial thin films. The schematic of the set up for MBE is shown in the Fig. 5.

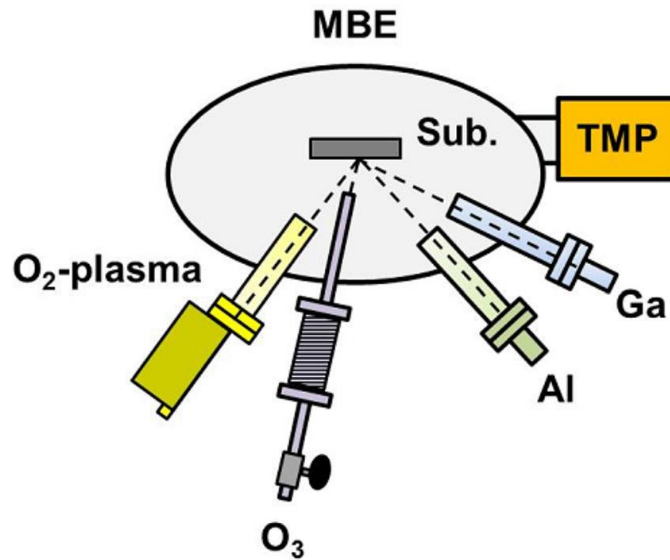

Figure 5: An MBE setup for Ga_2O_3 growth [28]

MBE growth uses two types of oxygen sources which are generated by rf-plasma cell [24-30] and ozone [31]. By adjusting the Ga cell temperature and oxygen flow rate ratio of O/Ga flux ratio is controlled.

In [28] successful growth of β-$(AlGa)_2O_3/Ga_2O_3$ hetero-structures have been reported. Based on the results it indicates that there will be a large scope of band gap engineering in Ga_2O_3 based materials system which leads to high performance heterostructure based electrical devices.

1.6.2 Metalorganic Chemical Vapor Deposition (MOCVD)

MOCVD is a thin film growth technique for several compound semiconductors for production of high quality films and mass production.

Ga_2O_3 crystals were grown by chemical reaction of trimethylgallium (TMGa) [38-40] or triethygallium (TEGa) [41] with H_2O or O_2. The typical growth temperatures are 600°C-850°C and the reported crystal quality of MOCVD grown Ga_2O_3 seems to be reasonably good. There were some stacking faults observed as crystallographic defects [38, 39, 41]. The major issue from MOCVD grown Ga_2O_3 thin films is poor control of electrical conductivity.

1.6.3 Halide vapor phase epitaxy (HVPE)

Out of all the growth methods, HVPE is the promising technique used for mass production of Ga_2O_3 epitaxial wafers because of its high speed, quality and thick Ga_2O_3 films with controlled electrical conductivity. Fig. 6 shows the schematic of the atmospheric-pressure HVPE system for Ga_2O_3 growth [33].

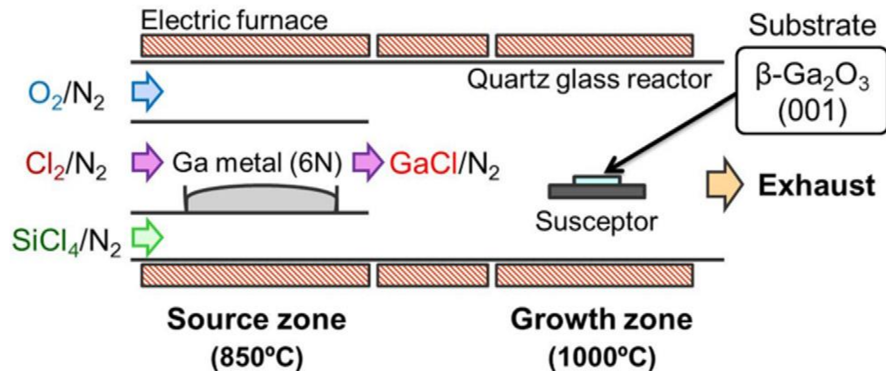

Figure 6: HVPE system for Ga_2O_3 growth [33]

For Ga_2O_3 growth, GaCl and O_2 are selected as precursors [33]. GaCl is formed by the reaction of high quality Ga metal and Cl_2 gas at 850ºC. N_2 is used as carrier gas and GaCl and O_2 are flowed into growth zone where Ga_2O_3 substrates are present. For n-type Ga_2O_3, $SiCl_4$ is used as dopant gas at 1000ºC. The highest growth rate recorded with excellent material and electrical properties of Ga_2O_3 films is about 20 μm per hour [33].

Oshima reported α- $Ga_2O_3$and β- Ga_2O_3 by growing hetero epitaxially on c-plane sapphire substrates through HVPE [35]. The growth rate recorded was 150 and 250μm per hour for α- Ga_2O_3 and β- Ga_2O_3 respectively [36]. This indicates that high quality Ga_2O_3 films were grown quickly using HVPE.

1.6.4 Mist-CVD

Mist-CVD is the simplest and cost-effective growth technique for Ga_2O_3 thin films. It is a method of vapor deposition process with mist particles which include precursors. Fig. 7 shows the schematic of the mist-CVD system.

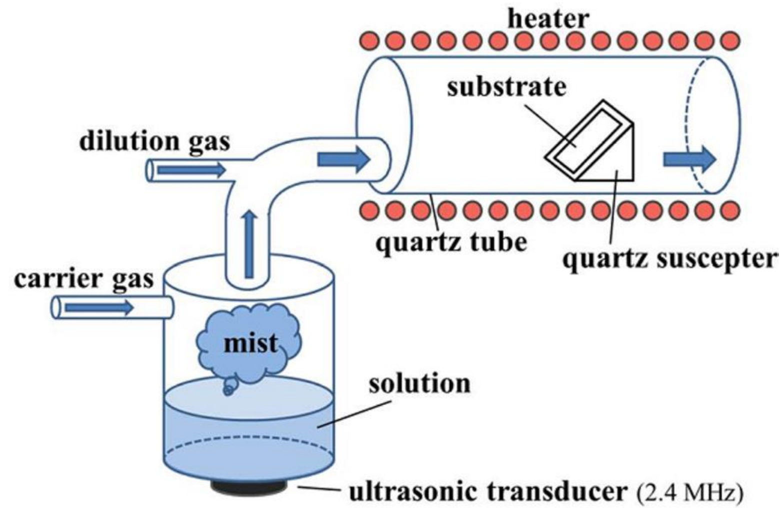

Figure 7: A Mist-CVD system for Ga_2O_3 growth [42]

The mist particles generated by source solution which is optimized by ultrasonic transducer are transferred to the growth chamber with help of a carrier gas.

c-plane sapphire is used as substrates. Carbon free gallium halides or carbon containing water solution of gallium acetylacetonate are used as gallium precursors. The concentration reported by Sn doping is in the range of 10^{17}-10^{19} cm^{-3} [42, 46].

Chapter 2

Experimental Techniques

In this chapter, a brief introduction of physical vapor deposition (PVD) is explained followed by detailed explanation of experimental techniques used in this research such as magnetron sputtering, rapid thermal processing (RTP), UV-VIS spectroscopy, x-ray diffraction and 4-point probe set up to find resistivity of thin films.

2.1 Physical Vapor Deposition

PVD is a method of deposition in which atoms of a material are vaporized from solid phase or liquid phase to vapor phase in the presence of high vacuum or low vacuum gaseous atmosphere. PVD is used to deposit thin films for optical, chemical, mechanical and electronic applications. Typically using PVD, thin films are deposited with thicknesses ranging from 10-100 μm [47].

The different types of PVD processes are [47]:

Sputter deposition:

Sputtering is a process of depositing thin films of a material onto the substrate. In the presence of generated plasma, the ions are forced onto the source material thereby eroding the source material in the form of individual atoms or molecules. Sputtering is further divided into high-pressure and low-pressure sputter deposition.

Vacuum evaporation:

In vacuum evaporation, the gas molecules in space between source and substrate are thermally evaporated without colliding.

Arc vapor deposition:

In Arc vapor deposition a high current electric arc and low voltage arc are used to erode the cathode electrode by moving arc to melt the anode electrode.

Ion plating:

In this method, atomic sized particles are bombarded to depositing film to change and control the properties of depositing film. In Ion plating arc vaporization or vacuum evaporation is used as source for depositing.

Fig.8 shows various PVD processes.

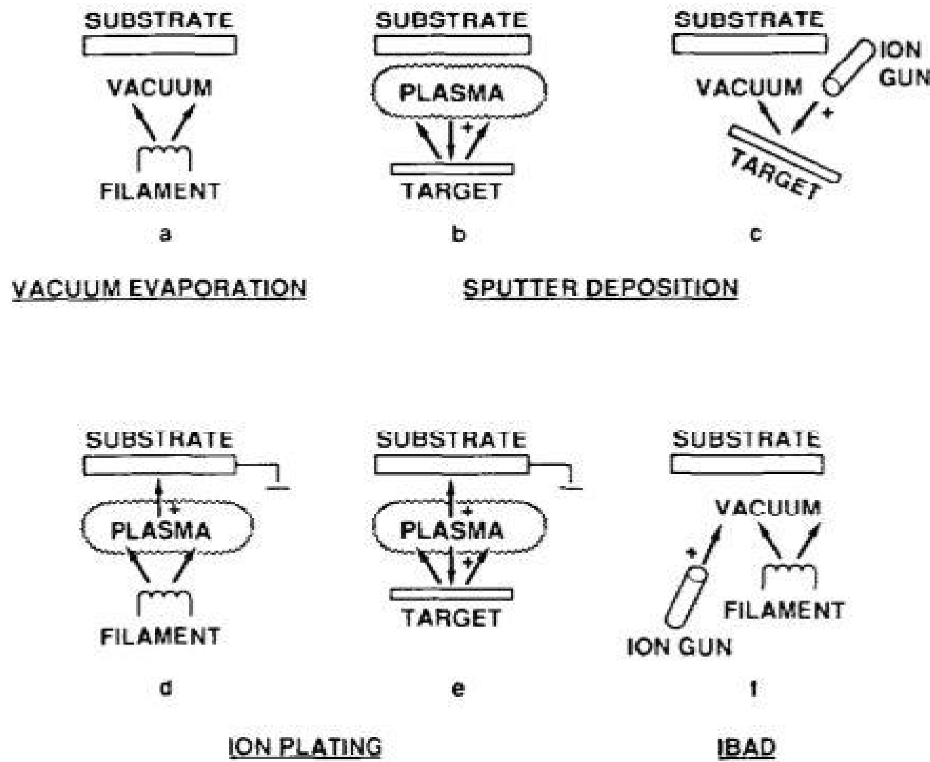

Figure 8: (a) Vacuum evaporation (b, c) Sputter deposition (d, e) Ion plating (f) IBAD [47]

2.2 Sputter Deposition

Sputter Deposition is a process of depositing particles onto the substrate placed in the vacuum chamber. The residual electrons, always present even in the best vacuum environment, are accelerated away from the negatively charged cathode and collides with and ionizes the argon gas atoms. The positively charged argon ions are attracted to the negatively charged cathode surface, colliding with it and eroding the source surface. These eroded atoms travel in straight lines and get deposited on the substrates placed over the target.

There are many factors that influence sputter yield. Some of them are energy, relative masses of ions, incident angle of bombarding ions and surface binding energy of source. There are various methods of sputtering which are widely used. They are ion beam and ion assisted sputtering, reactive sputtering and magnetron sputtering.

Magnetron sputtering is explained in detail in section 2.2.1 as it was used in fabrication of thin films in this research.

2.2.1 Magnetron Sputtering

Magnetron sputtering utilizes the magnets behind the cathode to attract the electrons over the negatively charged source. The electrons trapped in the presence of magnetic field boost the formation of ionization of gas molecules by multiple orders of magnitude. This increase in available ions leads to increase in the rate at which target material erodes and thereby increasing the deposition rate [49]. The magnetron sputter cathodes are usually circular or rectangular. Fig. 9 shows the process of magnetron sputter deposition.

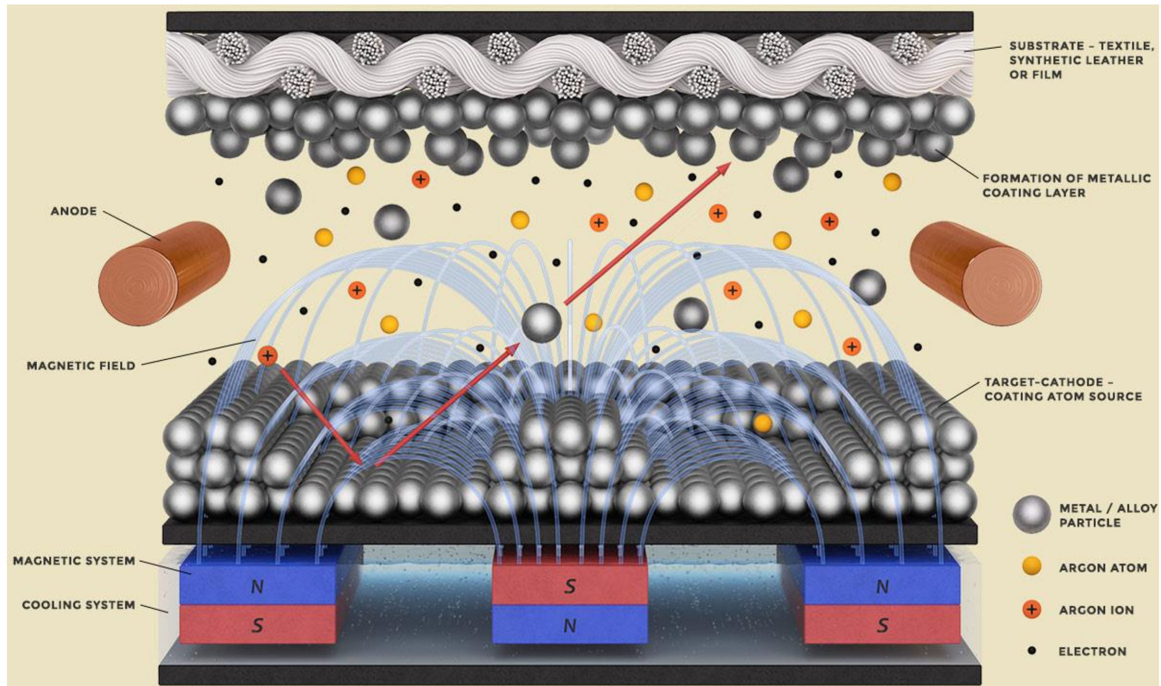

Figure 9: Magnetron sputtering mechanism [48]

2.3 Rapid Thermal Processing

Rapid thermal processing is a technique used frequently in semiconductor manufacturing to activate the dopants, change the phase or state of materials. This method is also used to enhance the properties like conductivity [49].

RTP is a process of heating samples at temperatures up to 1200°C on a time scale of several seconds or less in the required gas atmosphere. The samples are cooled down slowly to prevent dislocations and breakage due to rapid temperature difference.

Model RTP-300 rapid thermal processor used for this research which is shown in the Fig. 10.

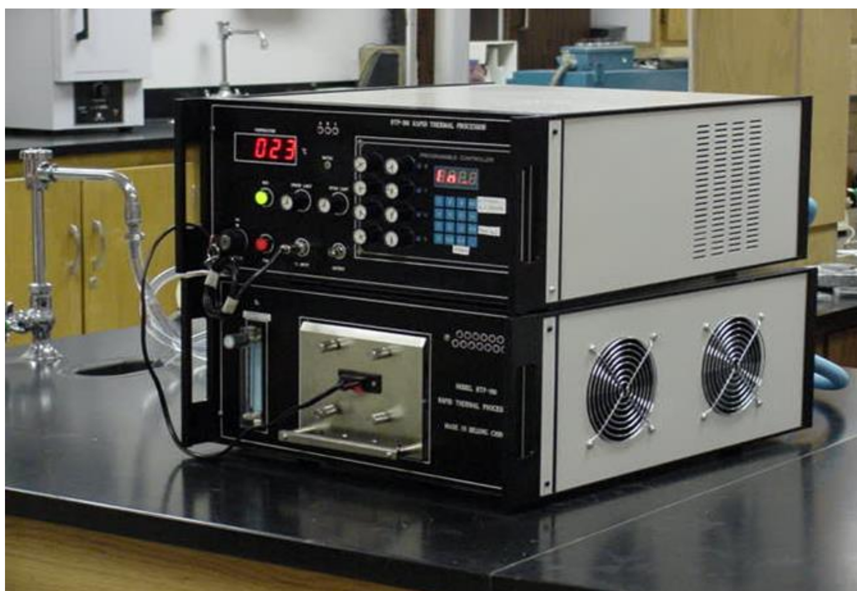

Figure 10: Rapid Thermal Processor

The deposited thin films in this investigation were placed on a silicon wafer which is placed in a quartz tube of the RTP. The annealing temperature and time were set by the programmable controller on the front panel of the RTP. The process gas is released at a controlled flow rate. Water cooling is provided to cool the system from overheating and prevent the tubes inside the system from melting. The temperature is maintained constant throughout the annealing process by adjusting the knobs of the controller. After completing the process of annealing, samples are cooled down to room temperature before shutting down the gas and water cooling systems.

2.4 Energy dispersive X-ray spectroscopy (EDS or EDX) using Scanning Electron Microscopy (SEM)

SEM produces images by scanning a beam of electrons on the sample. The incident beam of electrons interacts with the atoms of the sample and provide information

about the surface topography and elemental composition of the sample [51]. The resolution that can be achieved using SEM is more than 1 nm. Some of the main components of SEM are electron gun, lenses, electron detector and sample chamber. Fig.11 shows schematic of the SEM

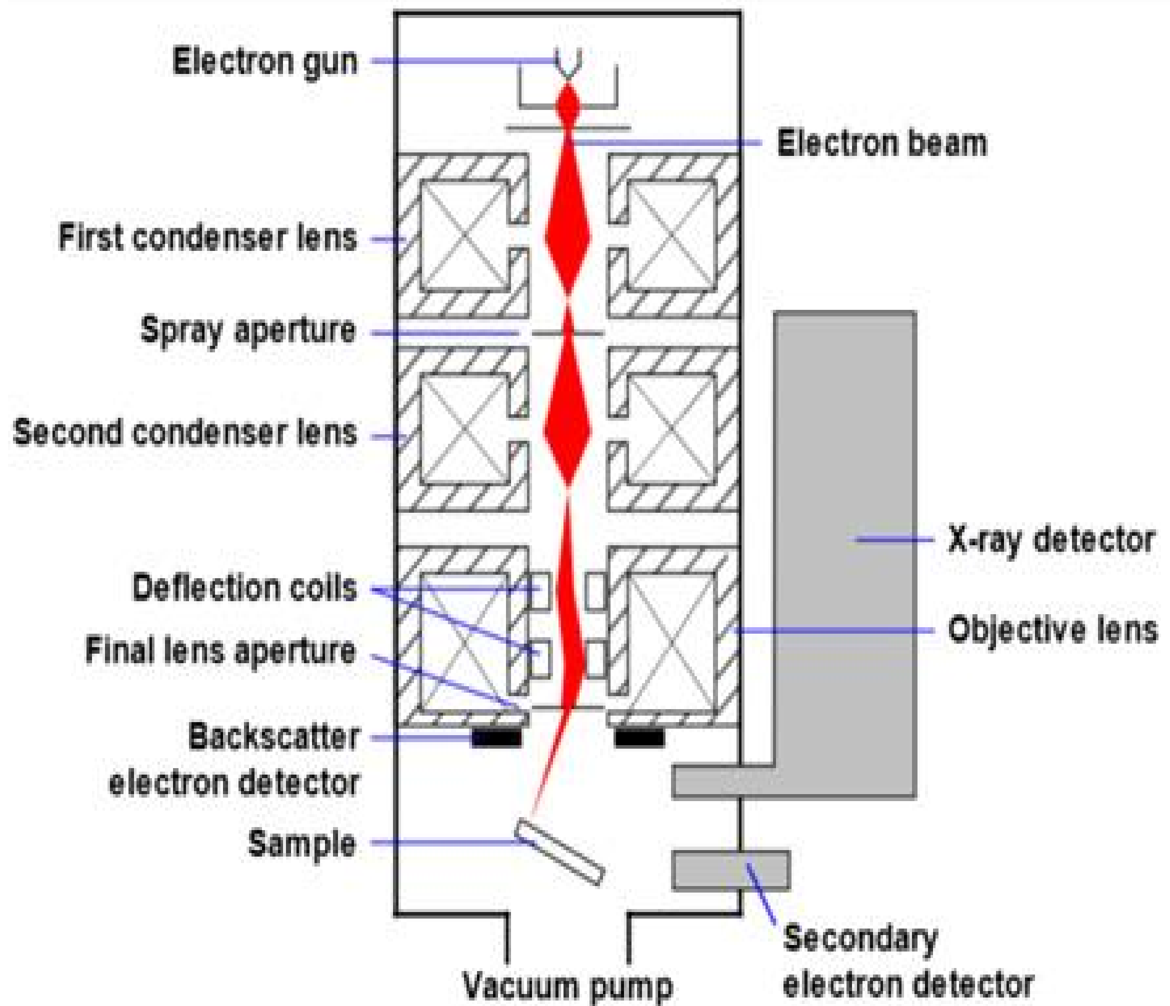

Figure 11: Schematic of SEM [50]

The electrons generated from the electron gun are accelerated down and passed through a series of lenses, coils and apertures to produce a focused beam of electrons on the sample. The vacuum pressure inside the sample and column chamber is maintained by

vacuum pumps. Various types of signals are produced when the electron beam interacts with atoms in the sample. They are

(a) **Secondary electrons (SE):** Secondary electrons are produced near to the surface of specimen. So, this signal helps in images up to a resolution of 1nm [51].

(b) **Back-scattered electrons (BSE):** BSE are generated due to reflection of electrons from sample due to elastic scattering. The images from BSE yield statistics about distribution of various elements in the sample [51].

(c) **Characteristic X-rays:** Characteristic x-rays are produced when the beam of electrons removes an electron from inner shell and filling the shell with high energy electron and release the energy (x-ray). The released energy provides information about the composition and measure of the element in the sample. This is the principle behind energy dispersive spectroscopy analysis [51].

Fig.12 shows the JOEL JSM-7600F scanning electron microscope used for this research.

Figure 12: JOEL JSM-7600F

2.5 X-ray Diffraction

X-ray diffraction is a non-destructive method utilized to identify the phase and unit cell dimensions of a crystalline material. It is the most common method used for crystal structures and the atomic spacing of thin films [52].

The basic principle of XRD is conditions satisfying Bragg’s law which relates the electromagnetic radiation to lattice spacing and angle of diffraction. Fig. 13 illustrates Bragg’s law.

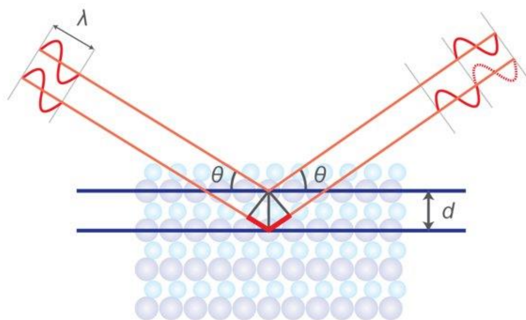

Figure 13: Bragg's law illustration [52]

$$n\lambda = 2d \sin \Theta$$

where n is an integer, λ is the characteristic wavelength of the incident x-ray on the sample, θ is the angle at which the X-rays are incident and d is the inter-planar spacing between rows of atoms.

The X-rays which are generated by a cathode ray tube are directed to the sample. So, when conditions satisfy Bragg's law, diffracted rays are produced. These diffracted rays are collected by the detector which is processed, and intensity is counted. The sample is scanned through a range of 2Θ angles and all diffraction rays of lattice are obtained [53].

Fig. 14 shows the BRUKER D8 prospector X-ray diffractometer used for this research. The major components in the diffractometer are X-ray tube to generate electrons, sample holder to mount the sample and a detector to acquire the diffracted rays from the sample.

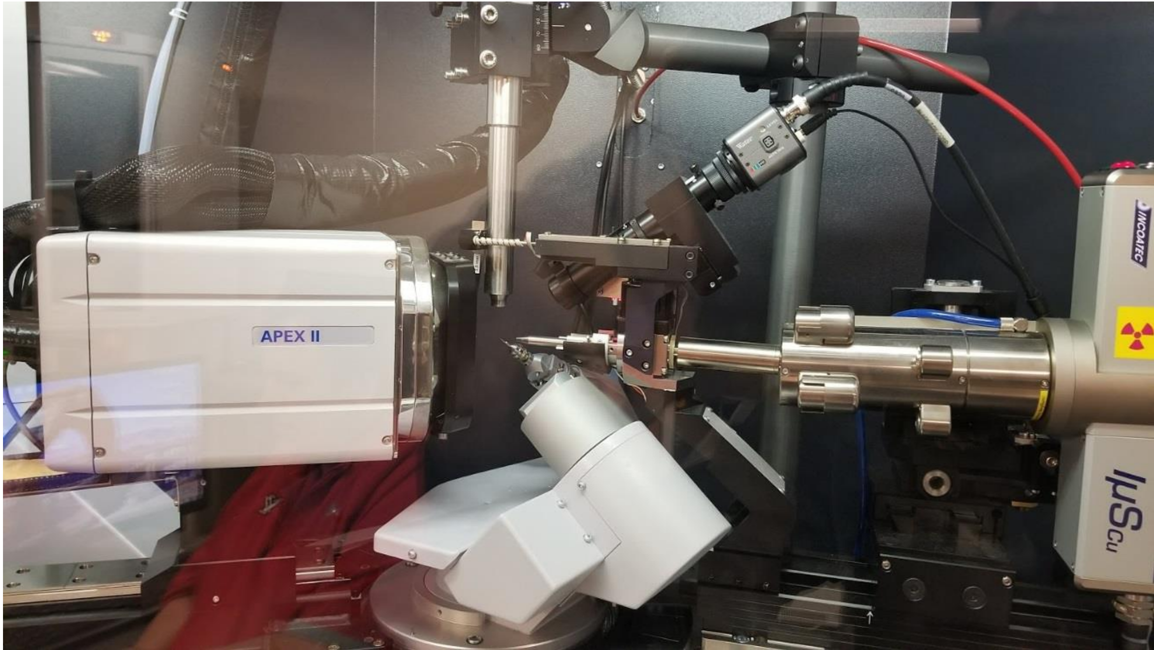

Figure 14: Bruker D8 Prospector close up

2.6 Four-point probe Resistivity Measurements

Four-point probe is a simple technique to determine the resistivity of a material, which is an important electrical property. It can be used for both bulk materials and thin films. The procedure and set up to find resistivity of thin films are briefly described here. Fig.15 shows the probe station, schematic and source meter used for resistivity measurements.

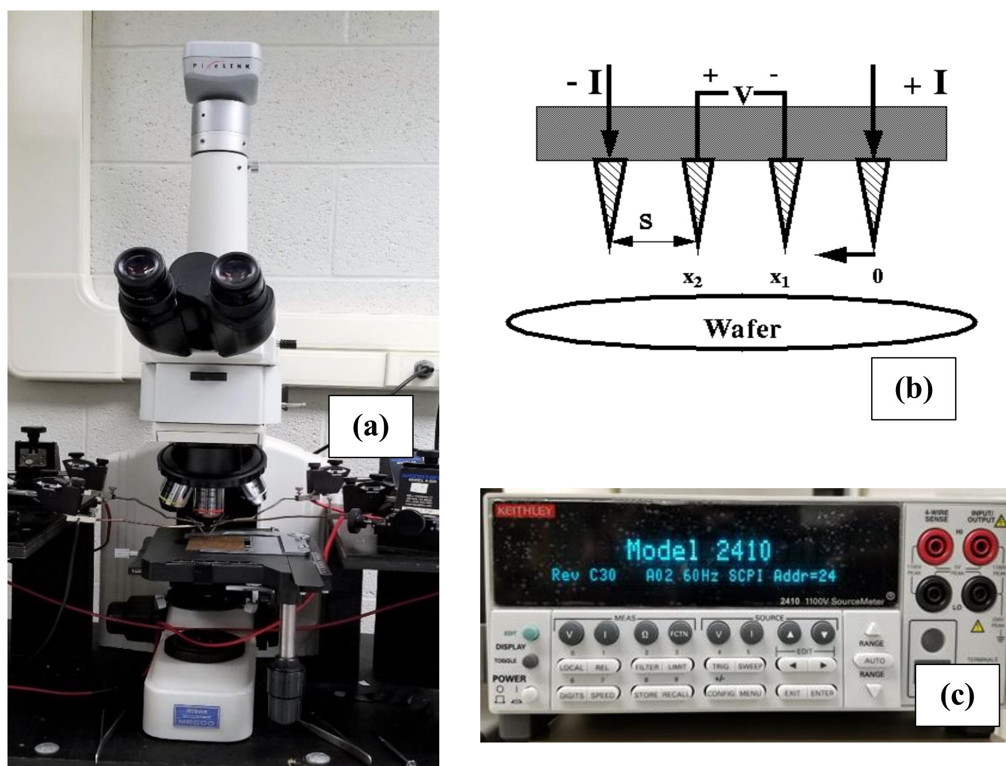

Figure 15: (a) Probe station (b) Schematic [54] (c) Keithley 2410 Source meter

Four probes with tungsten tips are equally spaced on the sample placed under the microscope stage as shown in Fig. 15 (a) and illustrated in Fig.15 (b). Current I is sourced through the outer probes and the voltage V is measured through the inner probes with Keithley 2410 Source meter show in Fig. 15 (c).

2.7 UV-Vis Spectroscopy

Transmission and absorbance measurements were analyzed using an Ocean Optics USB 4000-UV-Vis spectrometer, a deuterium/tungsten light source and spectra suite software to analyze the spectrometer data.

The light source emits light with wavelengths ranging from UV region (190 nm) to visible region (800 nm). The samples positioned across the path of light to record the

reference (sapphire substrate) and samples spectrums. The spectrometer collects the data of transmission and absorbance measurements individually and sends it to the spectra suite software to analyze the data. The schematic and equipment used for UV-Vis spectroscopy is shown in Fig. 16 and 17.

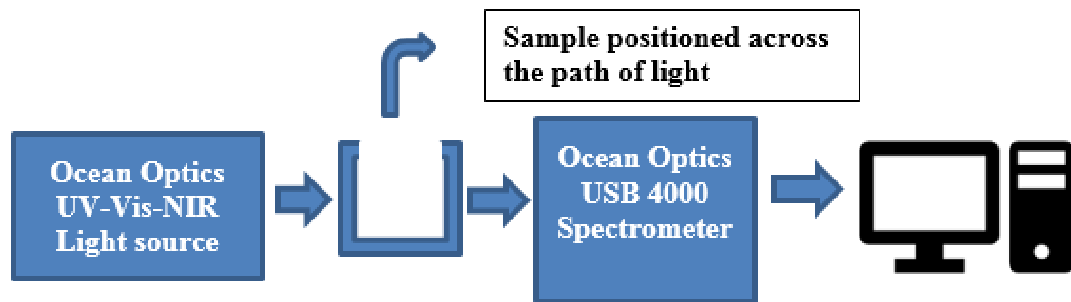

Figure 16: UV-Vis Spectroscopy set up

Figure 17: Ocean optics USB 4000 spectrometer and light source

Chapter 3

The Growth of Gallium Oxide Thin Films Using Magnetron Sputtering

All the thin films grown in this research were by magnetron sputtering. The principle of magnetron sputtering was explained earlier in Chapter 2. In this chapter the process and methodology to grow thin films by magnetron sputtering is explained.

Sputtering was performed in a deposition chamber as shown in Figure 18. The deposition chamber is a cylindrical glass bell jar enclosed in a cylindrical steel cage which is 18 inches in diameter and 28.5 inches in height. The main components in the sputtering deposition chamber are vacuum system, substrate heater, circular cathode electrodes, rf and dc power supplies, temperature controller, vent valve and mass flow controller. Fig. 19. shows the schematic of magnetron sputtering deposition chamber which is adapted from [55].

Figure 18: Sputter deposition chamber

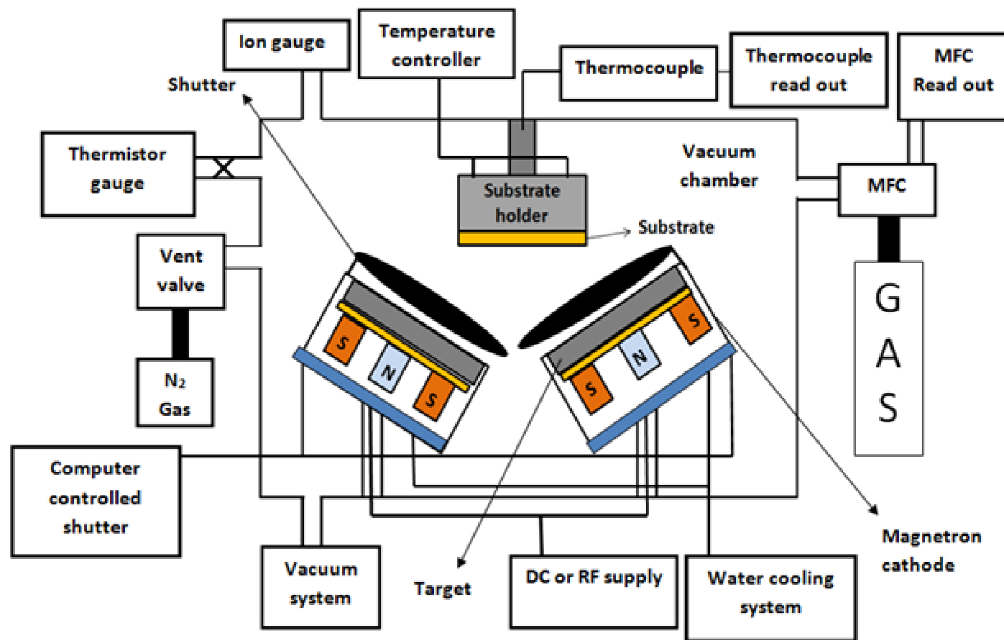

Figure 19: Schematic of magnetron sputter sputtering deposition chamber [adapted from 55]

3.1 Vacuum System

The vacuum required for sputter deposition is created and maintained by a combination of a mechanical pump and a turbo molecular pump. After the chamber is closed, the chamber is pumped down to 1 x 10^{-3} Torr by the mechanical pump. From there on the pressure is pumped down to low vacuum of 2 x 10^{-7} Torr by the turbo pump within 12 hours.

3.2 Substrate holder and heater

The substrate holder used provides heating up to about 1,000^{o}C. Fig. 20 shows the substrate holder and the heater with a double side sapphire substrate mounted on it.

Figure 20: Sapphire substrate mounted on heater

3.3 Target and Gun assembly

The gallium oxide target used in this research was purchased from Plasmaterials, Inc. and bonded to a copper backing plate. The tin target used for doping was purchased from Kurt J. Lesker, Inc. Both were 99.99 % pure and of diameter and thickness 2 inches and 0.125 inch respectively.

Fig. 21 (a) and (b) show pictures of the targets.

Figure 21: (a) Gallium oxide target (b) Tin target

The cathode “guns” used were purchased from Angstrom Sciences, Inc. The guns have flexible stems so that they can angled during co-deposition. Fig. 22 is a picture of the inside of the sputtering system showing the targets mounted on the cathodes.

Figure 22: Targets mounted on cathodes

3.4 Types of power supplies

3.4.1 Direct Current sputtering (DC)

Direct current sputtering is the basic and cost effective sputtering procedure for PVD metal deposition. It is commonly used in semiconductor industry to grow thin films onto the substrates. An output power of 500 W (0 to 600 V at 0 to 1 A) maximum is applied to the cathode. DC sputtering allows high current at low gas pressure (0.5 mTorr to 100 mTorr) to achieve a high thin film deposition rate. The limitation of DC sputtering is that it is economical for conducting materials for deposition. Deposition of non-conducting dielectric insulating materials cannot be achieved by DC sputtering.

Fig. 23 shows the DC power supply used in this research for metal deposition.

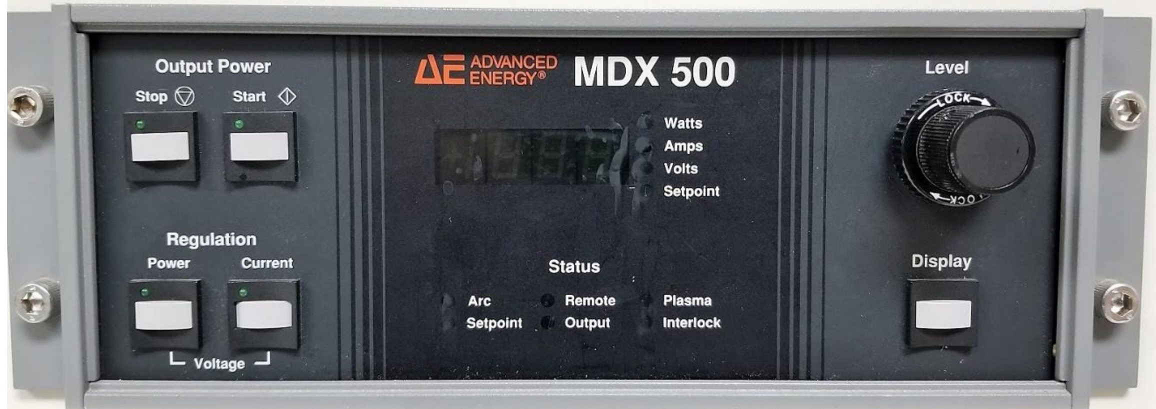

Figure 23: DC power supply

3.4.2 Radio Frequency Sputtering (RF)

RF sputtering is a technique where alternating electrical potential is applied in a vacuum environment at radio frequencies (13.56 MHz) to avoid charge build up on the sputter target materials. The charge buildup on the target material can be cleaned up with alternating the electrical potential. During the positive cycle, electrons are attracted to cathode giving it negative bias. During the negative cycle, positive ions collide with target which sputters it off and get deposited onto the substrate. Some of the dielectric materials which are commonly used in the semiconductor industry are aluminum oxide, silicon oxide and gallium oxide etc. Fig. 24 shows the RF power supply used to deposit thin films of Ga_2O_3 on c-sapphire substrate.

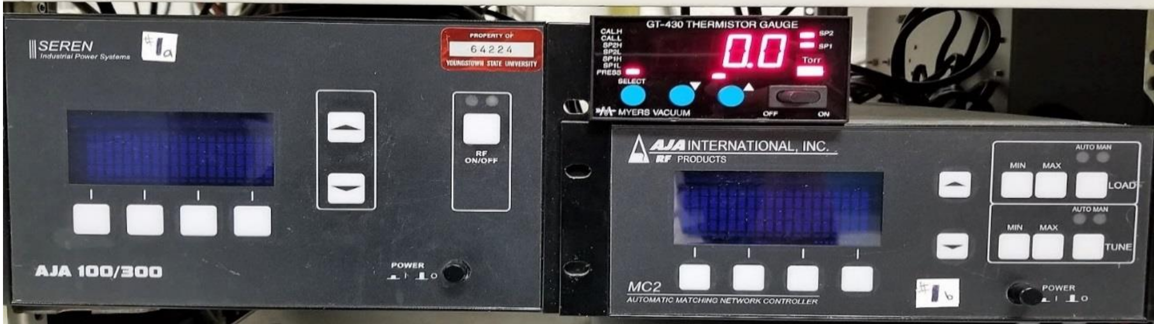

Figure 24: RF power supply

3.5 Temperature Controller and thermocouple

The temperature is controlled by a variac which is used to alter the voltage and current applied to the heating element. With this set-up, the sample can be heated up to 1000°C by increasing the temperature gradually. The thermocouple that is inserted into the substrate holder measures the temperature on the surface of the sample holder and displays the temperature digital reading on the thermocouple read out. Fig. 25 shows the digital thermocouple read out.

Figure 25: Thermocouple read out

3.6 Vent Valve and Mass Flow controller

Vent valve lets the deposition chamber to atmospheric pressure from the low vacuum. Regular dry nitrogen is used to vent the camber by opening the vent valve. A mass flow controller is used to control the flow rate of the process gas used for deposition. Fig. 26 shows the mass flow controller system.

Figure 26: Mass flow controller

3.7 Substrate cleaning and thermal desorption

Sample Cleaning: The substrates used for growth of gallium oxide thin films in this research were double-side polished c-plane sapphire which are 430 μm thick. Standard Radio Corporation of America (RCA) degreasing process is used to clean the substrates. This involves boiling the samples in acetone (3 min) followed by boiling in isopropyl alcohol (3 min) and finally rinsing the samples in de-ionized water. Fig 27 shows a cleaned double side sapphire substrate.

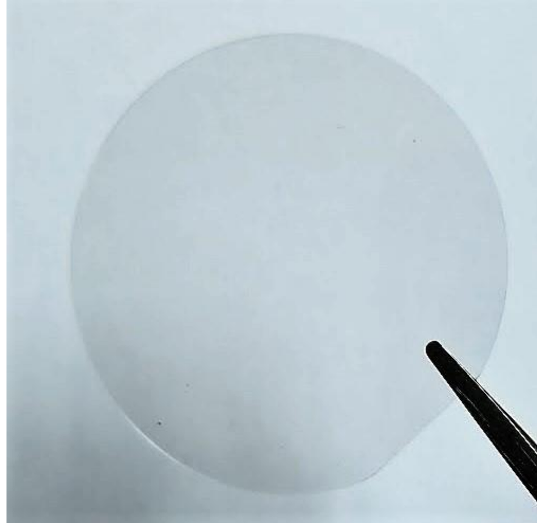

Figure 27: 3-inch c-plane sapphire substrate

Sample mounting: The samples were mounted on the heater as shown in Fig. 20. The Ga_2O_3 target was mounted on the circular cathode and fixed to hold the targets firmly as shown in Fig. 22.

Camber Pump down: The deposition chamber was evacuated to vacuum pressure about 10^{-7} Torr to remove contaminant gases.

Thermal Desorption: The substrates were pre-heated to clean, smooth and buffer the surface. Pre-heating provides a smaller RMS height when measured by AFM. This process offers a better surface to avoid the lattice mismatch between substrate and deposition material. Thermal desorption was done in O_2 gas atmosphere at 10mTorr pressure for 30 min at 700°C

Chapter 4

Results and Analysis

This chapter deals with the results of four investigations that were conducted in order to optimize the quality of the thin films First, the effect of different Ar/O_2 deposition gas composition of 100/0, 80/20, 50/50, 20/80 and 0/100 was investigated.. Second, the post deposition annealing was investigated where the films were annealed in vacuum and in different gas environments. Third, the substrate temperature was varied from 20^oC to 800^oC. The fourth investigation was where different amount of tin was introduced in order to perform n-type doping of the films. The films were analyzed by x-ray diffraction for physical and structural properties, energy dispersive spectroscopy for elemental compositions, UV-Vis spectroscopy for optical properties and four-point probe measurements to determine the resistivity of thin films.

4.1 Films deposited in gas mixtures of Argon (Ar) and Oxygen (O_2)

The c-plane sapphire substrates were cleaned by RCA process and thermal desorption was performed on substrate before the process of deposition as mentioned in section3.7. The temperature was then decreased to 500^oC for deposition of the thin films. Thin films were deposited in gases Ar 100/0, Ar/O_2 80/20, Ar/O_2 50/50, Ar/O_2 20/80 and O_2 100/0 separately at a flow rate of 10 standard cubic centimeters per minute (sccm) and 10 mTorr pressure at an RF power of 100 W for 2 hours. The thickness of the film was estimated to be about 200 nm.

4.1.1 X-ray Diffraction (XRD)

The Ga_2O_3 thin films deposited on c-plane sapphire substrate in different gas mixtures were run through an x-ray diffractometer to examine and characterize the physical and structural properties. Fig. 28 shows the XRD scans obtained from these β-Ga_2O_3 thin films.

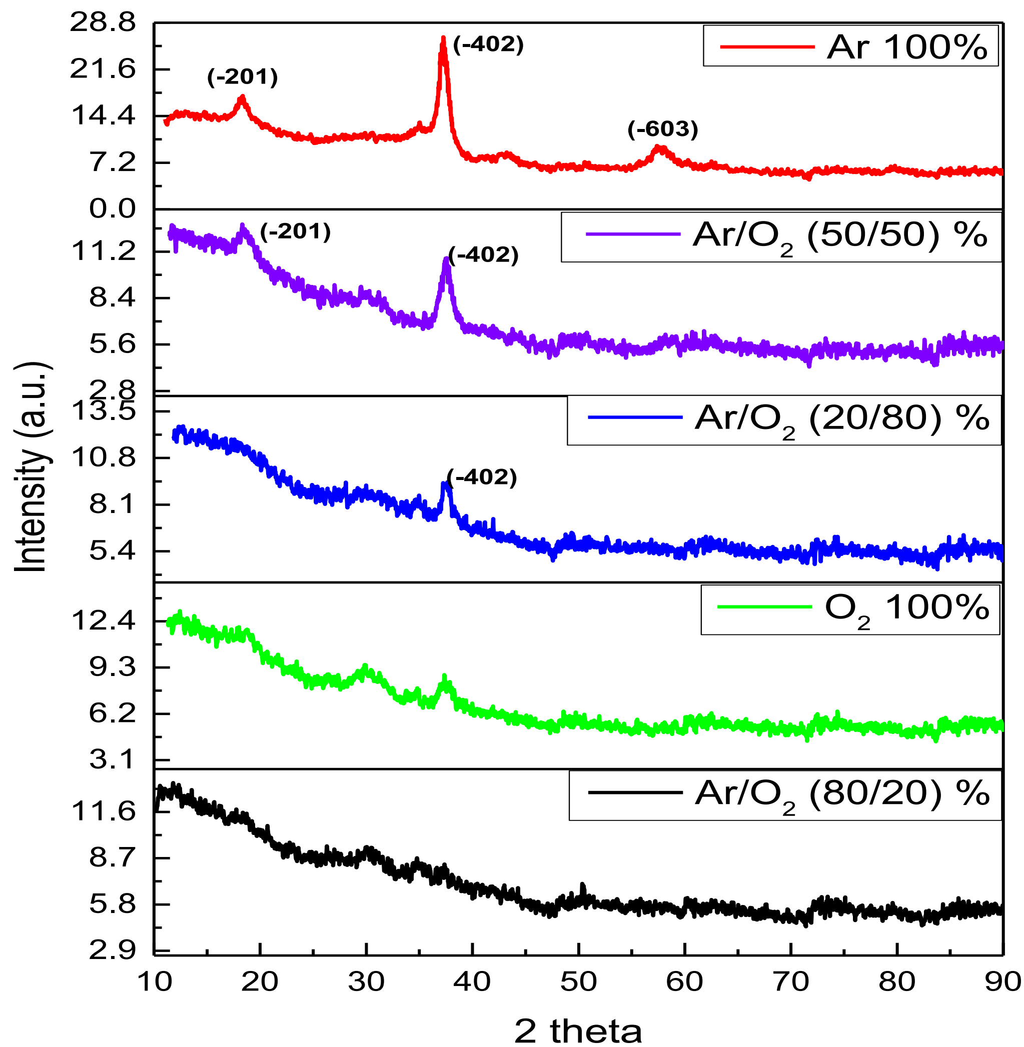

Figure 28: XRD data of films deposited in various gases

The films deposited in Ar/O_2 80/20 and 100% O_2 show no signs of crystalline nature whereas films deposited in Ar/O_2 20/80 and Ar/O_2 50/50 are crystalline in a very small fraction. But when films are deposited in 100% Ar, xrd scans display peaks at 18.9°, 38.4°, and 59.2° which correspond to diffractions of ($\bar{2}$ 0 1), ($\bar{4}$ 0 2) and ($\bar{6}$ 0 3) planes of β-Ga_2O_3. So, when films deposited in Ar 100% atmosphere at 500ºC there is a better formation of ($\bar{2}$ 0 1) oriented β-Ga_2O_3.

4.1.2 Energy dispersive Spectroscopy (EDS)

To determine the elemental composition in the deposited thin films, samples were run through EDS using SEM. Fig. 29 shows the elemental composition of films deposited in various gas proportions.

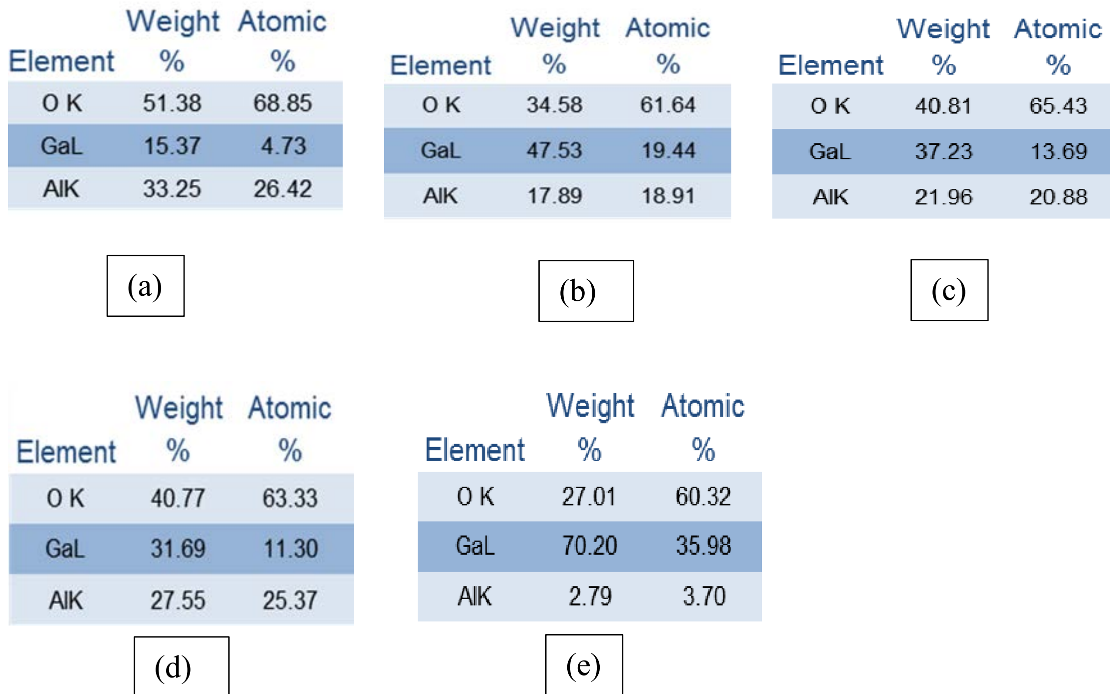

(a)

Element	Weight %	Atomic %
O K	51.38	68.85
GaL	15.37	4.73
AlK	33.25	26.42

(b)

Element	Weight %	Atomic %
O K	34.58	61.64
GaL	47.53	19.44
AlK	17.89	18.91

(c)

Element	Weight %	Atomic %
O K	40.81	65.43
GaL	37.23	13.69
AlK	21.96	20.88

(d)

Element	Weight %	Atomic %
O K	40.77	63.33
GaL	31.69	11.30
AlK	27.55	25.37

(e)

Element	Weight %	Atomic %
O K	27.01	60.32
GaL	70.20	35.98
AlK	2.79	3.70

Figure 29: EDS analysis on films deposited in (a) 100/0 O_2 (b) Ar/O_2 20/80 (c) Ar/O_2 50/50 (d) Ar/O_2 80/20 and (e) 100/0 Ar

EDS analysis results show that thin films deposited in 100% Ar has large atomic % of gallium content compared to other gas mixtures. The aluminum that shows up in the results is due to the Al content in sapphire substrate (Al_2O_3). Due to lack of calibration and also due to the oxygen contribution arising from the sapphire substrate, it is not possible to make a quantitative conclusion from the EDS data.

4.1.3 UV-Vis Spectroscopy

The optical characteristics were analyzed by UV-Vis spectroscopy. The transmission and absorbance of the deposited films were determined over the UV and visible range.

Transmission measurements

Fig. 30 shows the transmission results of films deposited in various gas proportions at 500°C. All the films were transparent and exhibited a transmission of 85-95% in the visible region.

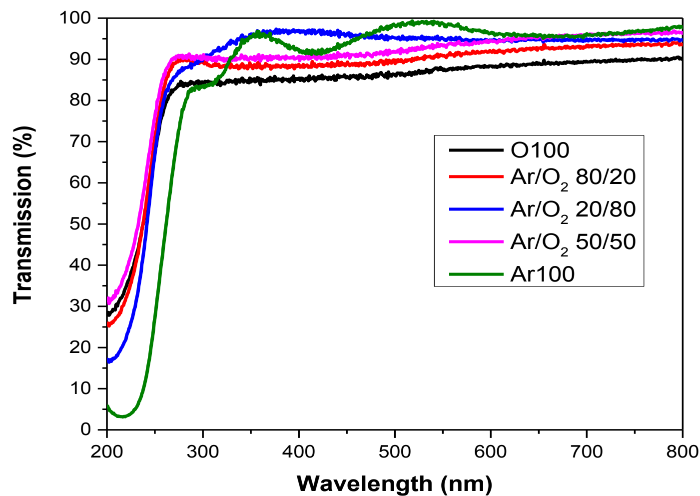

Figure 30: Transmission results of films deposited in various gases

Absorbance measurements

Fig. 31 shows the absorbance measurements of films deposited in various gas proportions at 500°C. The absorption of film deposited in 100% Ar starts at 280 nm and extends up to 340 nm while all other films show a cut-off absorption edge at 270nm.

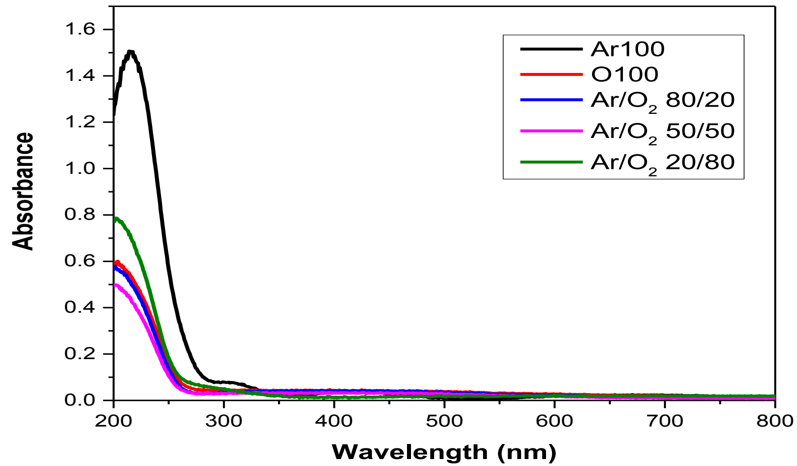

Figure 31: Absorbance results of films deposited in various gases

4.1.4 Optical bandgap

The optical bandgap energy (E_g) was estimated by UV-Vis spectroscopy result using Tauc plot [56]. The following relational expression is used in analysis of Optical band gap.

$$(h\nu\alpha)^{1/n} = B\,(h\nu - Eg)\ [56]$$

E_g is the bandgap, hν is the incident photo energy, , n is the nature of transition (n = 0.5 for direct transitions and n = 2 for indirect transitions) and B is the proportional constant and "α" is the absorption coefficient which is determines how far the light has travelled before being absorbed and is given by **$\alpha = 2.303\ A/t$ [56]**

A is the absorbance and t is the thickness of the deposited film. For Ga_2O_3 thin films, the nature of transition is 0.5 since it is direct band gap semiconductor and has direct transitions during recombination.

$$\mathbf{(h\nu\alpha)^2 = B\ (h\nu - Eg)}$$

From the above equation optical bandgap was determined by plotting graph between $(h\nu\alpha)^2$ vs photon energy(hν) and extrapolating the linear portions of $(h\nu\alpha)^2$ vs photon energy(hν) plot to $(h\nu\alpha)^2 = 0$ [56] as shown in Fig. 32 for the film deposited in 100% Ar.

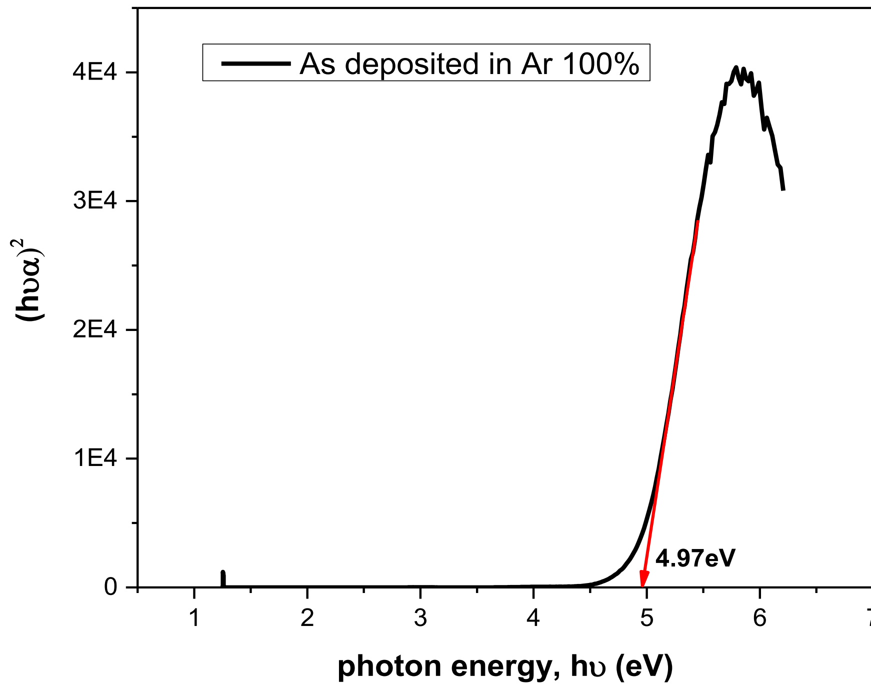

Figure 32: Tauc plot to determine optical bandgap

Table.2 shows the optical bandgap of the films deposited in different gases. The optical bandgap of film is less when deposited in Ar 100% and more when deposited in Ar/O_2 50/50.

Condition	Optical Bandgap (eV)
As deposited Gallium oxide in Ar 100%	4.97
As deposited Gallium oxide in O_2 100%	5.00
As deposited Gallium oxide in Ar/O_2 20/80	5.02
As deposited Gallium oxide in Ar/O_2 80/20	5.05
As deposited Gallium oxide in Ar/O_2 50/50	5.06

Table 2: Optical bandgap of Ga_2O_3 deposited in various gases

4.2 Annealing treatment on single crystal gallium oxide thin films

The single crystal gallium oxide thin films obtained by depositing in Ar 100/0 from first investigation are subjected to annealing. Annealing was performed in vacuum for 48 and 64 hours, N_2 at 1000°C for 1hour and Ar/O_2 80/20 at 900°C for 1 hour.

4.2.1 X-ray Diffraction (XRD)

All the single crystal Ga_2O_3 thin films annealed in various conditions are run through XRD to determine if there is any improvement in the crystal quality. Fig.33 shows the XRD scans of annealed single crystal thin films and also the as deposited single crystal thin film.

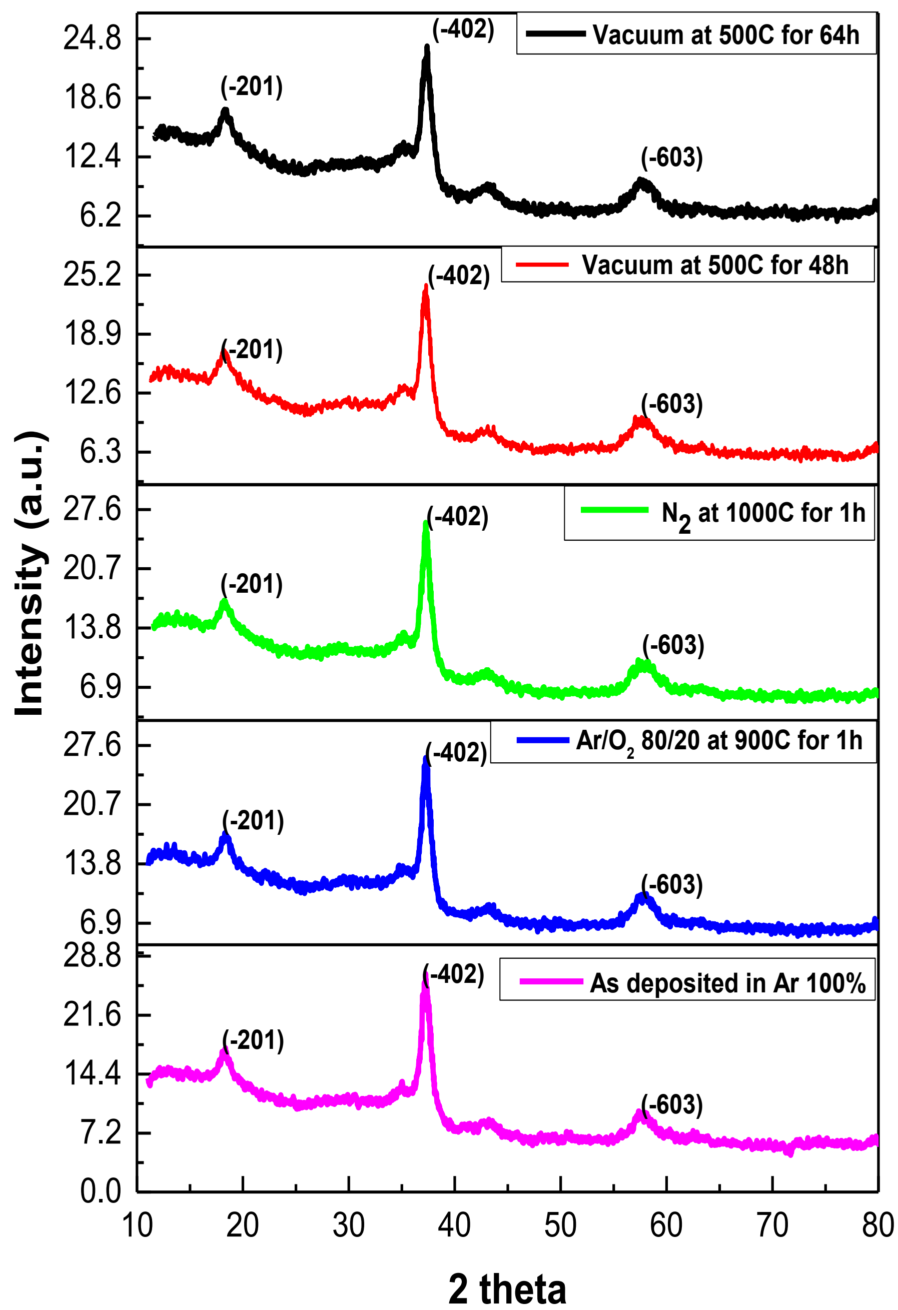

Figure 33: XRD data of single crystal thin Gallium oxide thin films annealed at various conditions

XRD data shows that there is no improvement in crystal quality of the β- Ga_2O_3 after annealing in the above conditions. All the samples represent single crystal β- Ga_2O_3 with ($\bar{2}$ 0 1) orientation.

4.2.2 Resistivity measurements

The four-point probe technique is widely used to determine the resistivity of the thin film. Four tungsten probes are equally spaced on the sample as shown in Fig. 15(b). Voltage V is sourced through the outer probes and the current I is measured through the inner probes with Keithley 2410 Source meter show in Fig. 15 (c).

For a thin film, the sheet resistivity (Ω-cm) is given by

$$\rho = (V/I)\ (\pi/\ln 2)\ t \quad [54]$$

I is the current measured and V is the voltage sourced. The factor ln 2 is used when t is the thickness of the film. The sheet resistance is given by

$$R = \rho/t = (V/I)\ (\pi/\ln 2) \quad [54]$$

The sheet resistivity and sheet resistance for thin film deposited in 100% Ar and annealed in vacuum for 64 hours is evaluated by sourcing a voltage of 18 mV and measured a current which is around 2 nA. So,

$$\text{Sheet resistivity } \rho = (18\text{mV}/2\text{nA})\ (\pi/\ln 2)\ 200\text{nm};\ \rho = 8.154\ \Omega\text{-cm}$$

$$\text{Sheet resistance } R = 4.07 * 10^5\ \Omega$$

The resistivity results show that thin film deposited in Ar and annealed in vacuum for 64 hours are highly resistive and show no signs of conductivity. The efforts to evaluate resistivity on the other thin films was not successful as the values of current are so low (in the range of nA – pA) which are affected by noise.

4.2.3 Optical bandgap

Optical bandgap was determined by process explained in section 4.1.4. Table.3 shows the calculated optical bandgaps of films annealed at various conditions.

Table 3: Optical bandgap of annealed single crystal thin films

Conditions	Optical Bandgap (eV)
As deposited	4.97
Annealed in N_2 at 1000C for 1hr	4.93
Annealed in Ar/O_2 80/20 at 950C for 1 hr	4.86
Annealed in vacuum at 500C for 64h	4.94

Optical bandgap reduces with annealing the thin films. The optical bandgap of the un-annealed sample is 4.97 which is more than the annealed samples. This decrease in optical bandgap is due to a very little increase in the lattice constants because of annealing.

4.3 Ga_2O_3 films deposited at various substrate temperatures in Ar/O_2 80/20

The c-plane sapphire substrates were cleaned by RCA process and thermal desorption was performed on substrate before the process of deposition as mentioned in section3.7. Thin films were deposited in gases Ar/O_2 80/20 separately at a flow rate of 10 standard cubic centimeters per minute (sccm) and 10mTorr pressure at an RF power of 200W for 2hours at substrate temperatures 20^oC, 250^oC, 500^oC, 650^oC and 800^oC. . The thickness of the film was estimated to be about 200 nm.

4.3.1 X-ray Diffraction

The Ga_2O_3 thin films deposited on sapphire substrate at various substrate temperatures were run through an x-ray diffractometer to examine and characterize the structural properties.

Fig. 34 shows the XRD scans obtained from these Ga_2O_3 films.

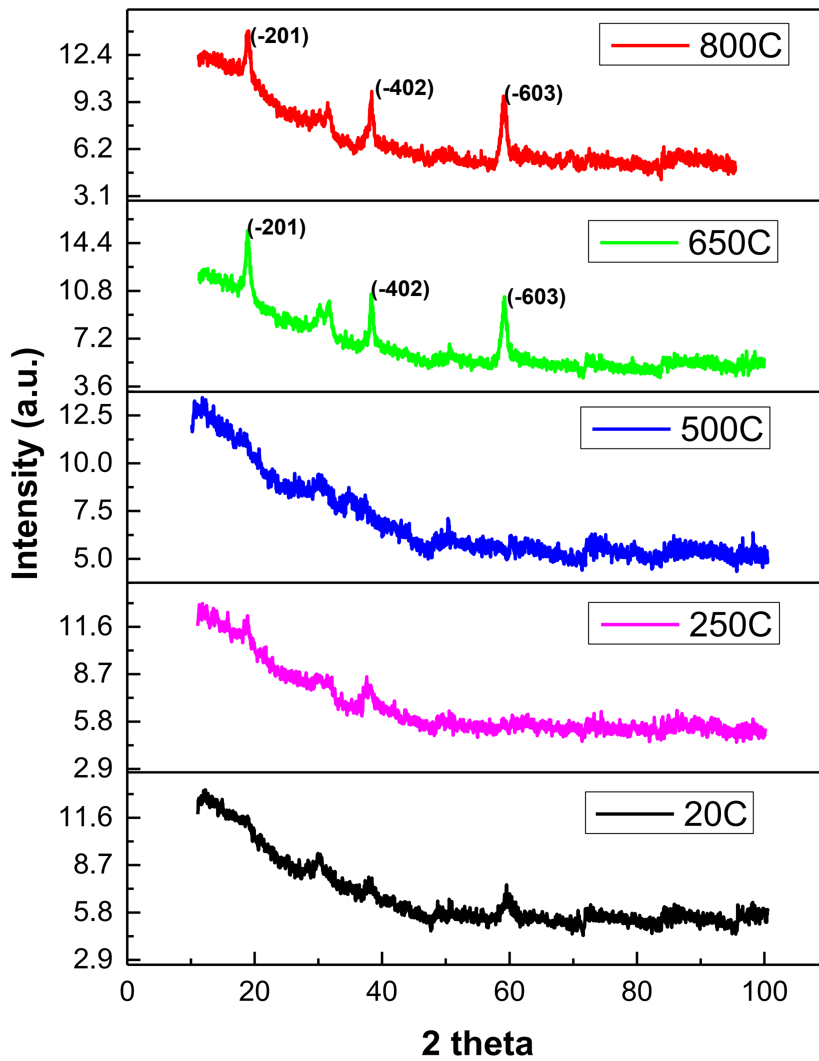

Figure 34: XRD data of films deposited at various temperatures

The films deposited at 20ºC, 250ºC and 500ºC show no signs of formation single crystal Ga_2O_3. The peaks at 18.9°, 38.4°, and 59.2° in 650ºC and 800ºC samples correspond to diffractions of ($\bar{2}$ 0 1), ($\bar{4}$ 0 2) and ($\bar{6}$ 0 3) planes of β-Ga_2O_3. The films start crystallizing when substrate temperatures are above 500ºC. The sample deposited at 800ºC show better formation of ($\bar{2}$ 0 1) oriented β-Ga_2O_3.

4.3.2 Energy dispersive Spectroscopy (EDS)

To determine the elemental composition of the films deposited at various temperatures, the samples were run through EDS using SEM. Fig.35 shows the EDS results of the films deposited at various substrate temperatures.

(a)

Element	Weight %	Atomic %
O K	54.84	71.79
GaL	14.39	4.32
AlK	30.77	23.89

(b)

Element	Weight %	Atomic %
O K	40.08	63.95
GaL	35.59	13.03
AlK	24.33	23.02

(c)

Element	Weight %	Atomic %
O K	37.42	64.49
GaL	45.41	17.96
AlK	17.17	17.54

(d)

Element	Weight %	Atomic %
O K	39.99	63.10
GaL	33.58	12.16
AlK	26.44	24.74

(e)

Element	Weight %	Atomic %
O K	44.13	66.24
GaL	29.26	10.08
AlK	26.61	23.69

Figure 35: Films deposited in Ar/O_2 80/20 at various substrate temperatures (a) 20ºC (b) 250ºC (c) 500ºC (d) 650ºC and (e) 800ºC

4.3.3 UV- Vis Spectroscopy

Transmission measurements

Fig. 36 shows the transmission results of films deposited in various substrate temperatures. All the films were transparent and exhibited a transmission of 85-95% in the visible region.

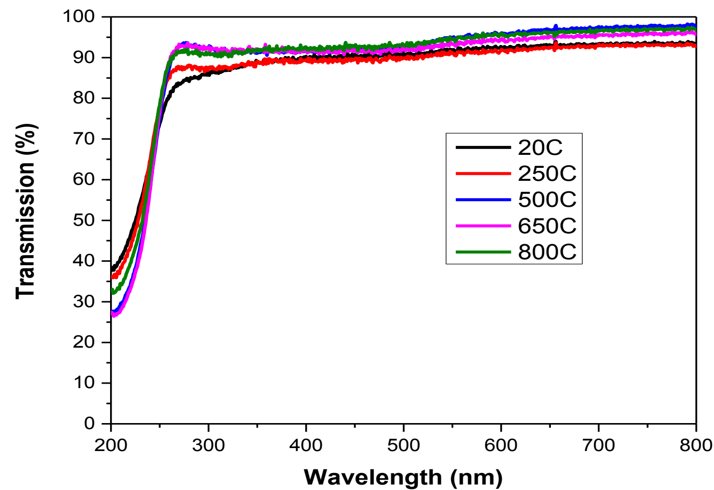

Figure 36: Transmission measurements on films deposited at various temperatures

Absorbance measurements

Fig.37 shows the absorbance measurements of films deposited at various gas temperatures. The absorption edge of all the films was around 260-270nm.

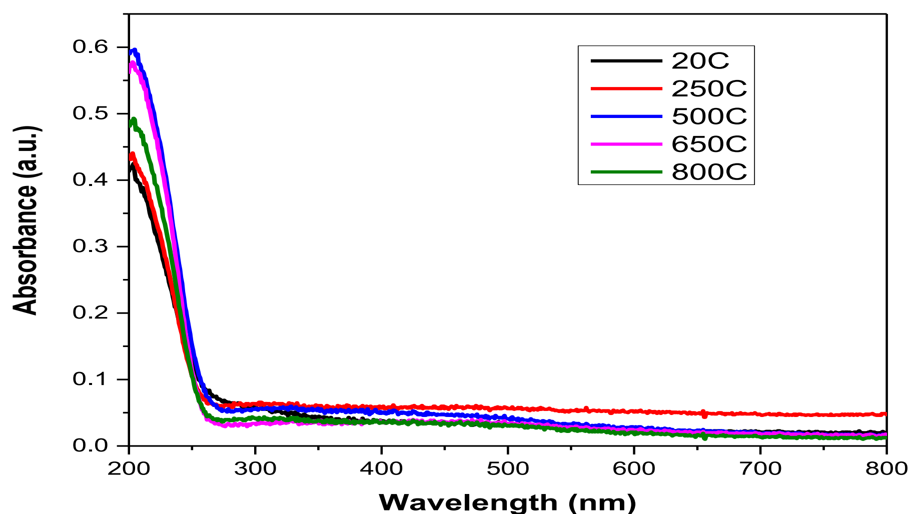

Figure 37: Absorbance measurements on films deposited at various temperatures

4.3.4 Optical Bandgap

Optical bandgap was determined by process explained in section 4.1.4. The films deposited at substrate temperature of 500ºC has the least bandgap of 5.04 eV and more when deposited at 20ºC which is 5.09 eV. Table.4 compares the optical bandgaps of films deposited at various substrate temperatures.

Table 4: Optical bandgap of Ga_2O_3 deposited in various temperatures

Condition	Optical Bandgap (eV)
As deposited Gallium oxide in Ar/O_2 80/20 at 20C	5.09
As deposited Gallium oxide in Ar/O_2 80/20 at 250C	5.07
As deposited Gallium oxide in Ar/O_2 80/20 at 500C	5.04
As deposited Gallium oxide in Ar/O_2 80/20 at 650C	5.06
As deposited Gallium oxide in Ar/O_2 80/20 at 800C	5.06

4.4 Annealing in different gas atmospheres of 800 nm thick Gallium oxide film

The c-plane sapphire substrates were cleaned by RCA process and thermal desorption was performed on substrate before the process of deposition as mentioned in section3.7. Thin films were deposited in Ar/O_2 50/50 gas at 700^oC with a flow rate of 10 standard cubic centimeters per minute (sccm) and 10 mTorr pressure at an rf power of 200 W for 12 hours (4 hour per day to over avoid heating the cathode). The expected thickness of the thin films is 800 nm.

Annealing was performed in Ar, Ar/O_2 50/50, O_2 and N_2 gas atmospheres at 900^oC for 3 min by rapid thermal processor (RTP) which is explained in section 2.3.

4.4.1 X-ray Diffraction (XRD)

The samples annealed in various gases along with un-annealed (UA) sample was run through XRD for structural properties.

Fig. 38 shows the scans of the films annealed in various gases.

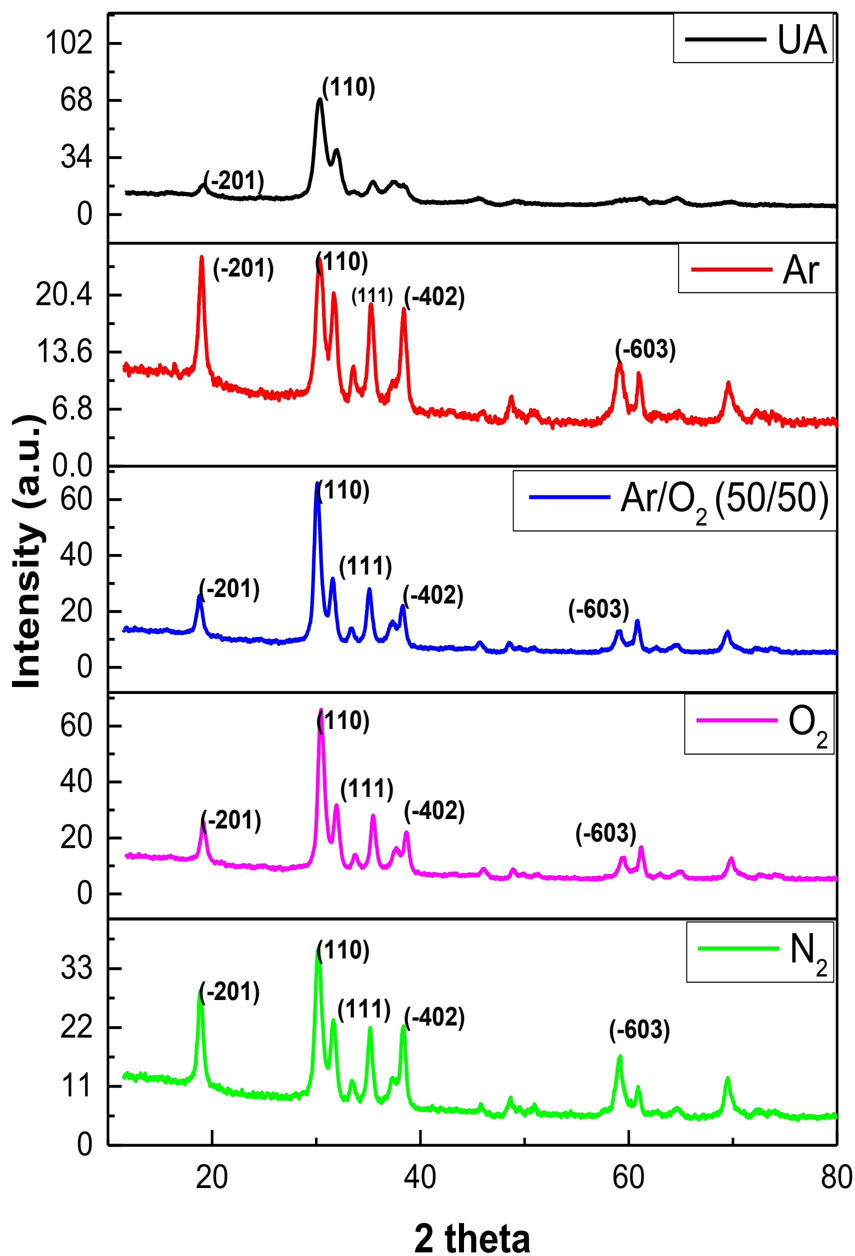

Figure 38: XRD data of films annealed in various gases

All the samples represented poly-crystalline structure and did not show any increase in intensity when annealed in different gases.

4.5 Doping Gallium oxide (Ga_2O_3) thin films with Tin (Sn)

Ga_2O_3 has a wide range of elements for doping from group-IV elements out of which Sn has been most promising dopant and less activation energy. Sn substitutes Ga atom and forms a 4+ oxidation state which results in a free electron in Ga_2O_3 lattice. This phenomenon increases the carrier concentration and hence the conductivity.

In this investigation, different amount of tin was introduced in order to perform n-type doping of the films. The c-plane sapphire substrates were cleaned by RCA process as mentioned in section3.7. Doping was performed in Ar atmosphere with a flow rate of 10 standard cubic centimeters per minute (sccm) and 10 mTorr pressure at 500^oC for 6 hours 30 minutes.

Sn doping was performed by simultaneously depositing Ga_2O_3 and Sn on to the substrate. Different amount of Sn was introduced into the thin films by maintaining deposition power (225 W) Ga_2O_3 constant and varying deposition power of Sn (0.008 A, 0.020 A and 0.025 A). The cathodes are angled in such a way that both Ga_2O_3 and Sn are deposited simultaneously on to the substrate. Fig. 19 shows the schematic for uniform doping of Ga_2O_3 with Sn.

4.5.1 EDS measurements

EDS measurements were conducted on the samples with different Sn deposition power to evaluate the elemental composition and concentration of Sn in the doped samples.

(a) Condition 1

Deposition power of Sn: 0.008 A (DC power)

Deposition power of Ga_2O_3: 225 W (RF power)

Element	Weight %	Atomic %	Net Int.	Error %	Kratio	Z	R
O K	18.62	50.75	881.03	7.50	0.12	1.34	0.87
GaL	74.96	46.89	2,401.24	3.15	0.63	0.93	1.03
SnL	6.42	2.36	83.55	11.73	0.05	0.8	1.1

(b) Condition 2

Deposition power of Sn: 0.020 A (DC power)

Deposition power of Ga_2O_3: 225 W (RF power)

Element	Weight %	Atomic %	Net Int.	Error %	Kratio	Z	R
O K	22.42	56.96	854.59	7.37	0.15	1.32	0.87
GaL	68.43	39.90	1,662.32	3.48	0.55	0.92	1.04
SnL	9.15	3.14	93.41	9.64	0.07	0.79	1.11

(c) Condition 3

Deposition power of Sn: 0.025 A (DC power)

Deposition power of Ga_2O_3: 225 W (RF power)

Element	Weight %	Atomic %	Net Int.	Error %	Kratio	Z	R
O K	20.07	53.60	854.73	7.46	0.13	1.34	0.87
GaL	69.74	42.73	1,922.35	3.48	0.57	0.93	1.03
SnL	10.18	3.66	118.12	8.59	0.08	0.8	1.1

EDS analysis results show that the at. % of Sn in doped thin films with deposition powers of 0.008 A, 0.020 A and 0.025 A is 2.3%, 3.1% and 3.6% respectively. The at. % of Sn in the thin films increased with increase in deposition power in the process of deposition.

4.5.2 XRD measurements

The doped samples were run through XRD to determine the structural properties. Fig. 40 shows the XRD scans obtained from Sn doped Ga_2O_3 films.

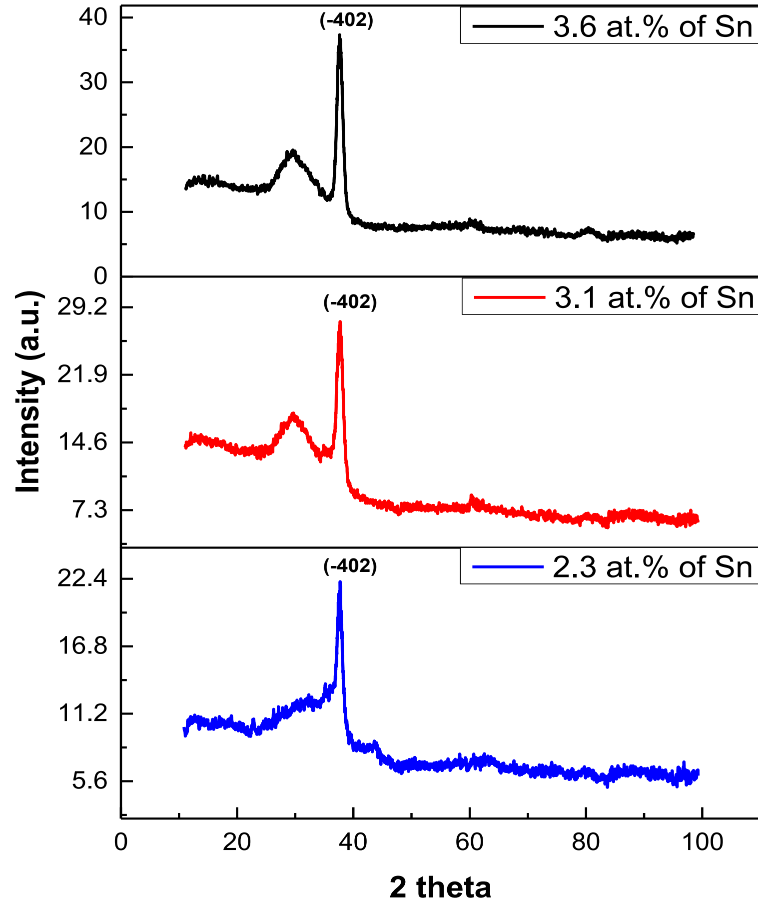

Figure 39: XRD data of Ga_2O_3: Sn samples

A peak which showed up at 29.4° of 3.1 at. % and 3.6 at. % of Sn in the thin films. The peak corresponds to the formation of defects due to increase in the concentration of Sn. The peaks at 38.4° in the doped films correspond to diffraction of ($\bar{4}$ 0 2) plane of ($\bar{2}$ 0 1) oriented β-Ga_2O_3.

4.5.3 Optical characteristics

The transmission and absorbance of the Ga_2O_3 films doped with various proportions of Sn are characterized using UV-Vis spectroscopy.

Transmission measurements

Fig.41 shows the transmission measurements of doped films. All the films despite of doping showed transmission of 80-90% in the visible region. The effect of doping on the transparency of thin films is less.

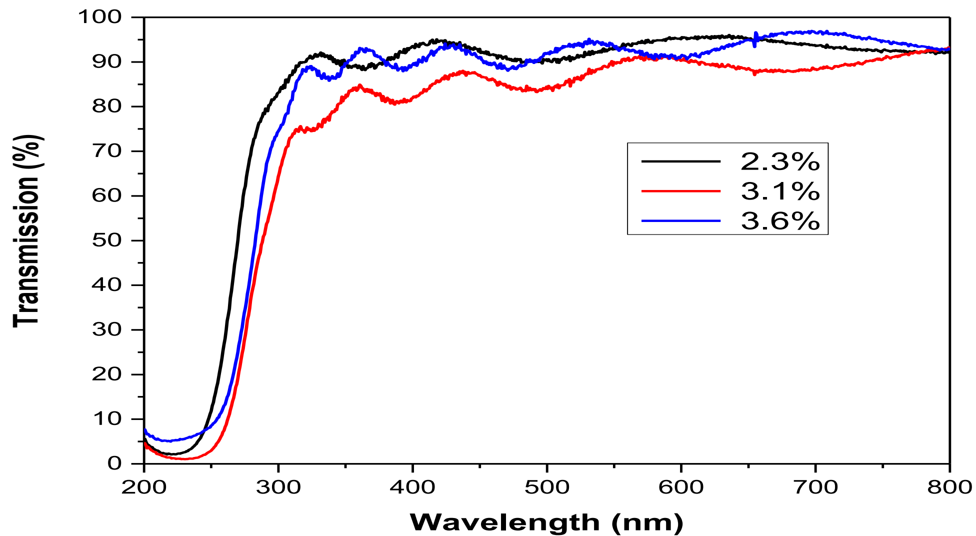

Figure 40: Transmission measurements of uniformly doped samples

Absorbance measurements

Fig.42 shows the absorbance results of Ga_2O_3 films doped with Sn. The absorption of the doped films was around 300nm. The absorption edge of doped films was increased by 30 nm to that of undoped thin films which is around 270nm.

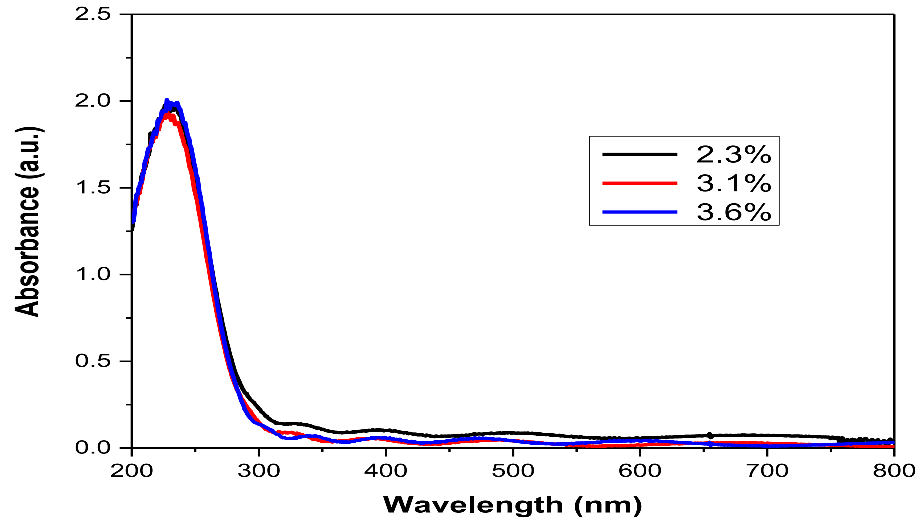

Figure 41: Absorbance measurements of uniformly doped samples

4.5.4 Optical Bandgap

Optical bandgap was determined by process explained in section 4.1.4. Table. 5 shows the optical bandgap of Ga_2O_3 films doped with Sn.

Table 5: Optical bandgap of Ga_2O_3 : Sn

Condition	Optical Band gap (eV)
2.3 at.% of Sn	4.65
3.1 at.% of Sn	4.61
3.6 at.% of Sn	4.58

The optical bandgap decreases with increase in the concentration of Sn in the thin films. The observed decrease in the bandgap could be due to the substitution of Ga with Sn. The ionic radius of Sn (0.225 nm) is slightly larger that Ga (0.122 nm), thereby leading to increase in the lattice constant and decrease in optical bandgap.

Chapter -5

Conclusions and future work

5.1 Conclusion

Gallium oxide thin films were fabricated on c-plane sapphire substrates by rf magnetron sputtering The first investigation involved films were deposited in gases Ar 100/0, Ar/O_2 80/20, Ar/O_2 50/50, Ar/O_2 20/80 and O_2 100/0 at a substrate temperature of 500°C. XRD data revealed peaks at 18.9°, 38.4°, and 59.2° which correspond to ($\bar{2}$ 0 1), ($\bar{4}$ 0 2) and ($\bar{6}$ 0 3) oriented β-Ga_2O_3 single crystal thin film was obtained when deposited in Ar atmosphere. UV-Vis spectroscopy showed transmission of 90-95% and optical band gaps of 4.9eV-5.0 eV. In the second investigation, annealing was performed on single crystal Ga_2O_3 thin films in N_2, Ar/O_2 80/20 over 950°C for 1 hour and in vacuum for 48 hours and 64hours at 500°C. XRD data showed no growth in intensity for formation of β-Ga_2O_3 and optical band gap is approximately 4.8-4.9eV. Optical bandgap results revealed that annealing improves the lattice parameters and decreases the band energy. The third investigation involved films deposited at different substrate temperatures ranging from 20C to 800C in Ar/O_2 80/20. XRD data showed that high temperatures (650°C and 800°C) yield a better formation of β-Ga_2O_3. Gallium oxide thin films deposited in Ar/O_2 (50/50) at 700C and post annealing the samples in N_2, O_2, Ar and Ar/O_2 50/50 gas atmospheres at 900°C for 3 min represented a poly crystalline structure. The final investigation was where uniform doping was performed with 2.3at. %, 3.1at. %, 3.6at. % concentrations of tin (Sn). XRD data showed that increase in the concentration of Sn to Ga_2O_3 films leads to defects. Also, addition of Sn dopants in the

thin films produced a decrease in the optical bandgap with increase in the concentration of Sn to the films.

5.2 Future work

The parameters in process of annealing such as temperature, gas and time should be optimized to achieve better quality of single crystal Ga_2O_3 thin films. Sn which is the most promising element for doping Ga_2O_3 thin films could be advanced to improve the conductivity of the thin films. A UV-C photodetector, photodiode and a solar panel could be fabricated once the thin films shown signs of good conductivity.

References

[1] G. E. Moore, "Cramming more components onto integrated circuits, Reprinted from Electronics, volume 38, number 8, April 19, 1965, pp.114 ff.," *IEEE Solid-State Circuits Society Newsletter*, vol. 11, no. 3, pp. 33–35, Sep. 2006

[2]"Transistor count," *Wikipedia*. 29-Mar-2018.

[3] L. Dong, R. Jia, B. Xin, B. Peng, and Y. Zhang, "Effects of oxygen vacancies on the structural and optical properties of β-Ga_2O_3," *Scientific Reports*, vol. 7, p. 40160, Jan. 2017

[4] R. Roy, V. G. Hill, and E. F. Osborn, "Polymorphism of Ga_2O_3 and the System Ga_2O_3—H_2O," *J. Am. Chem. Soc.*, vol. 74, no. 3, pp. 719–722, Feb. 1952

[5] S.-D. Lee, K. Akaiwa, and S. Fujita, "Thermal stability of single crystalline alpha gallium oxide films on sapphire substrates," *Phys. Status Solidi C*, vol. 10, no. 11, pp. 1592–1595, Nov. 2013.

[6] C. Janowitz *et al.*, "Experimental electronic structure of In 2 O 3 and Ga 2 O 3," *New J. Phys.*, vol. 13, no. 8, p. 085014, 2011.

[7] K. Shimamura, E. G. Víllora, T. Ujiie, and K. Aoki, "Excitation and photoluminescence of pure and Si-doped β- Ga_2O_3 single crystals," *Appl. Phys. Lett.*, vol. 92, no. 20, p. 201914, May 2008.

[8] Z. Galazka, K. Irmscher, R. Uecker, R. Bertram, M. Pietsch, A. Kwasniewski, M. Naumann, T. Schulz, R. Schewski and D. Klimm "On the bulk β- Ga_2O_3 single crystals grown by the Czochralski method," *Journal of Crystal Growth*, vol. 404, pp. 184–191, Oct. 2014.

[9] T. Harwig, F. Kellendonk, and S. Slappendel, "The ultraviolet luminescence of β-galliumsesquioxide," *Journal of Physics and Chemistry of Solids*, vol. 39, no. 6, pp. 675–680, Jan. 1978.

[10] "Solid State Communications | Vol 7, Issue 24, Pages 1739-1835 (15 December 1969) | ScienceDirect.com." [Online]. Available: https://www.sciencedirect.com/journal/solid-state-communications/vol/7/issue/24. [Accessed: 28-Feb-2018].

[11] T. Harwig and F. Kellendonk, "Some observations on the photoluminescence of doped β-galliumsesquioxide," *Journal of Solid State Chemistry*, vol. 24, no. 3, pp. 255–263, Apr. 1978.

[12] J. B. Varley, J. R. Weber, A. Janotti, and C. G. Van de Walle, “Oxygen vacancies and donor impurities in β-Ga2O3,” *Appl. Phys. Lett.*, vol. 97, no. 14, p. 142106, Oct. 2010.

[13] R. Stevenson, “Gallium Oxide: Power Electronics’ Cool New Flavor,” 30-Mar-2016. [Online]. Available: https://spectrum.ieee.org/semiconductors/materials/gallium-oxide-power-electronics-cool-new-flavor. [Accessed: 02-Mar-2018].

[14] N. Ueda, H. Hosono, R. Waseda, and H. Kawazoe, “Synthesis and control of conductivity of ultraviolet transmitting β- Ga_2O_3 single crystals,” *Appl. Phys. Lett.*, vol. 70, no. 26, pp. 3561–3563, Jun. 1997.

[15] E. G. Víllora, K. Shimamura, Y. Yoshikawa, T. Ujiie, and K. Aoki, “Electrical conductivity and carrier concentration control in β- Ga_2O_3 by Si doping,” *Appl. Phys. Lett.*, vol. 92, no. 20, p. 202120, May 2008

[16] K. Irmscher, Z. Galazka, M. Pietsch, R. Uecker, and R. Fornari, “Electrical properties of β- Ga_2O_3 single crystals grown by the Czochralski method,” *Journal of Applied Physics*, vol. 110, no. 6, p. 063720, Sep. 2011.

[17] S. Ohira, M. Yoshioka, T. Sugawara, K. Nakajima, and T. Shishido, “Fabrication of hexagonal GaN on the surface of β- Ga_2O_3 single crystal by nitridation with NH3,” *Thin Solid Films*, vol. 496, no. 1, pp. 53–57, Feb. 2006.

[18] A. Kuramata, K. Koshi, S. Watanabe, Y. Yamaoka, T. Masui, and S. Yamakoshi, “High-quality β- Ga_2O_3 single crystals grown by edge-defined film-fed growth,” *Jpn. J. Appl. Phys.*, vol. 55, no. 12, p. 1202A2, Nov. 2016

[19] Y. Tomm, P. Reiche, D. Klimm, and T. Fukuda, “Czochralski grown Ga_2O_3 crystals,” *Journal of Crystal Growth*, vol. 220, no. 4, pp. 510–514, Dec. 2000.

[20] Z. Galazka, Uecker R, Klimm D, Irmscher K, Naumann M, Pietsch M, Kwasniewski A, Bertram R, Ganschow S and Bickermann “Scaling-Up of Bulk β- Ga_2O_3 Single Crystals by the Czochralski Method,” *ECS J. Solid State Sci. Technol.*, vol. 6, no. 2, pp. Q3007–Q3011, Jan. 2017.

[21] K. Hoshikawa, E. Ohba, T. Kobayashi, J. Yanagisawa, C. Miyagawa, and Y. Nakamura, “Growth of β- Ga_2O_3 single crystals using vertical Bridgman method in ambient air,” *Journal of Crystal Growth*, vol. 447, pp. 36–41, Aug. 2016.

[22] H. Aida, K. Nishiguchi, H. Takeda, N. Aota, K. Sunakawa, and Y. Yaguchi, “Growth of β- Ga_2O_3 Single Crystals by the Edge-Defined, Film Fed Growth Method,” *Jpn. J. Appl. Phys.*, vol. 47, no. 11R, p. 8506, Nov. 2008.

[23] K. Sasaki, A. Kuramata, T. Masui, E. G. Víllora, K. Shimamura, and S. Yamakoshi, “Device-Quality β- Ga_2O_3 Epitaxial Films Fabricated by Ozone Molecular Beam Epitaxy,” *Appl. Phys. Express*, vol. 5, no. 3, p. 035502, Feb. 2012.

[24] E. G. Víllora, K. Shimamura, K. Kitamura, and K. Aoki, “Rf-plasma-assisted molecular-beam epitaxy of β- Ga_2O_3,” *Appl. Phys. Lett.*, vol. 88, no. 3, p. 031105, Jan. 2006.

[25] T. Oshima, T. Okuno, and S. Fujita, “Ga_2O_3 Thin Film Growth on c-Plane Sapphire Substrates by Molecular Beam Epitaxy for Deep-Ultraviolet Photodetectors,” *Jpn. J. Appl. Phys.*, vol. 46, no. 11R, p. 7217, Nov. 2007.

[26] H. Okumura, M. Kita, K. Sasaki, A. Kuramata, M. Higashiwaki, and J. S. Speck, “Systematic investigation of the growth rate of β- Ga_2O_3 (010) by plasma-assisted molecular beam epitaxy,” *Appl. Phys. Express*, vol. 7, no. 9, p. 095501, Aug. 2014.

[27] P. Vogt and O. Bierwagen, “The competing oxide and sub-oxide formation in metal-oxide molecular beam epitaxy,” *Appl. Phys. Lett.*, vol. 106, no. 8, p. 081910, Feb. 2015.

[28] S. W. Kaun, F. Wu, and J. S. Speck, “β-$(AlG_{1-x})_2O_3$ (010) heterostructures grown on β-Ga2O3 (010) substrates by plasma-assisted molecular beam epitaxy,” *Journal of Vacuum Science & Technology A: Vacuum, Surfaces, and Films*, vol. 33, no. 4, p. 041508, Jun. 2015.

[29] P. Vogt and O. Bierwagen, “Reaction kinetics and growth window for plasma-assisted molecular beam epitaxy of Ga_2O_3: Incorporation of Ga vs. Ga_2O desorption,” *Appl. Phys. Lett.*, vol. 108, no. 7, p. 072101, Feb. 2016.

[30] P. Vogt and O. Bierwagen, "Kinetics versus thermodynamics of the metal incorporation in molecular beam epitaxy of (InxGa1−x)$_2$O$_3$," *APL Materials*, vol. 4, no. 8, p. 086112, Aug. 2016

[31] K. Sasaki, M. Higashiwaki, A. Kuramata, T. Masui, and S. Yamakoshi, "Growth temperature dependences of structural and electrical properties of Ga_2O_3 epitaxial films grown on β- Ga_2O_3 (010) substrates by molecular beam epitaxy," *Journal of Crystal Growth*, vol. 392, pp. 30–33, Apr. 2014.

[32] T. Matsumoto, M. Aoki, A. Kinoshita, and T. Aono, "Absorption and Reflection of Vapor Grown Single Crystal Platelets of β- Ga_2O_3," *Jpn. J. Appl. Phys.*, vol. 13, no. 10, p. 1578, Oct. 1974.

[33] "Thermodynamic study of β- Ga_2O_3 growth by halide vapor phase epitaxy - ScienceDirect." [Online].
Available: https://www.sciencedirect.com/science/article/pii/S0022024814004369?via%3Dihub. [Accessed: 02-Mar-2018]

[34] H. Murakami, Hisashi, Kazushiro Nomura, Ken Goto, Kohei Sasaki, Katsuaki Kawara, Quang Tu Thieu, Rie Togashi "Homoepitaxial growth of β- Ga_2O_3 layers by halide vapor phase epitaxy," *Appl. Phys. Express*, vol. 8, no. 1, p. 015503, Dec. 2014.

[35] Y. Oshima, E. G. Víllora, and K. Shimamura, “Halide vapor phase epitaxy of twin-free α- Ga_2O_3 on sapphire (0001) substrates,” *Appl. Phys. Express*, vol. 8, no. 5, p. 055501, Apr. 2015.

[36] Y. Oshima, E. G. Víllora, and K. Shimamura, “Quasi-heteroepitaxial growth of β-Ga2O3 on off-angled sapphire (0001) substrates by halide vapor phase epitaxy,” *Journal of Crystal Growth*, vol. 410, pp. 53–58, Jan. 2015.

[37] C.-Y. Huang, R.-H. Horng, D.-S. Wuu, L.-W. Tu, and H.-S. Kao, “Thermal annealing effect on material characterizations of β- Ga_2O_3 epilayer grown by metal organic chemical vapor deposition,” *Appl. Phys. Lett.*, vol. 102, no. 1, p. 011119, Jan. 2013

[38] G. Wagner, Baldini M, Gogova D, Schmidbauer M, Schewski R, Albrecht M, Galazka Z, Klimm D and Fornari “Homoepitaxial growth of β- Ga_2O_3 layers by metal-organic vapor phase epitaxy,” *Phys. Status Solidi A*, vol. 211, no. 1, pp. 27–33, Jan. 2014.

[39] D. Gogova, G.Wagner, M.Baldini, M.Schmidbauer, K.Irmscher, R.Schewski, Z.Galazka, M.Albrecht, R.Fornari “Structural properties of Si-doped β- Ga_2O_3 layers grown by MOVPE,” *Journal of Crystal Growth*, vol. 401, pp. 665–669, Sep. 2014.

[40] M. J. Tadjer, Michael A. Mastro, Nadeemullah A. Mahadik, Marc Currie,Virginia D. Wheeler, Jaime A. FreitasJr., Jordan D. Greenlee,

Jennifer K. Hite, Karl D. Hobart, Charles R. EddyJr., Fritz J. Kub, "Structural, Optical, and Electrical Characterization of Monoclinic β- Ga_2O_3 Grown by MOVPE on Sapphire Substrates," *Journal of Elec Materi*, vol. 45, no. 4, pp. 2031–2037, Apr. 2016.

[41] M. Baldini, M. Albrecht, D. Gogova, R. Schewski, and G. Wagner, "Effect of indium as a surfactant in $(Ga_{1-x}In_x)_2O_3$ epitaxial growth on β - Ga_2O_3 by metal organic vapour phase epitaxy," *Semicond. Sci. Technol.*, vol. 30, no. 2, p. 024013, 2015.

[42] T. Kawaharamura, G. T. Dang, and M. Furuta, "Successful Growth of Conductive Highly Crystalline Sn-Doped α- Ga_2O_3 Thin Films by Fine-Channel Mist Chemical Vapor Deposition," *Jpn. J. Appl. Phys.*, vol. 51, no. 4R, p. 040207, Mar. 2012.

[43] K. Kaneko, K. Suzuki, Y. Ito, and S. Fujita, "Growth characteristics of corundum-structured α-$(AlxGa1-x)_2O_3$/ Ga_2O_3 heterostructures on sapphire substrates," *Journal of Crystal Growth*, vol. 436, pp. 150–154, Feb. 2016

[44] R. Jinno, T. Uchida, K. Kaneko, and S. Fujita, "Reduction in edge dislocation density in corundum-structured α- Ga_2O_3 layers on sapphire substrates with quasi-graded α-$(Al,Ga)_2O_3$ buffer layers," *Appl. Phys. Express*, vol. 9, no. 7, p. 071101, Jun. 2016

[45] M. Oda, K. Kaneko, S. Fujita, and T. Hitora, "Crack-free thick (~5 μm) α-Ga2O3 films on sapphire substrates with α-$(Al,Ga)_2O_3$ buffer layers," *Jpn. J. Appl. Phys.*, vol. 55, no. 12, p. 1202B4, Oct. 2016.

[46] K. Akaiwa, K. Kaneko, K. Ichino, and S. Fujita, “Conductivity control of Sn-doped α- Ga_2O_3 thin films grown on sapphire substrates,” *Jpn. J. Appl. Phys.*, vol. 55, no. 12, p. 1202BA, Nov. 2016.

[47] “Handbook of Physical Vapor Deposition (PVD) Processing - (Second Edition) - ScienceDirect.” [Online].
Available: https://www.sciencedirect.com/science/book/9780815520375. [Accessed: 19-Apr-2018]

[48] “Technology · Farotex.” [Online]. Available: http://farotex.com/technology.html. [Accessed: 28-Apr-2018].

[49] Gade, R. R. (2015). Comparison of delta and uniform doped p-type and n-type ZnO films (Youngstown State University).

[50] “How an SEM works.” [Online].
Available: https://www.nanoscience.com/technology/sem-technology/how-sem-works/. [Accessed: 18-Apr-2018].

[51] “Scanning electron microscope,” *Wikipedia*. 08-Mar-2018.

[52] “X-ray diffraction | Rigaku.” [Online].
Available: https://www.rigaku.com/en/techniques/xrd. [Accessed: 18-Apr-2018].

[53] "X-ray Powder Diffraction (XRD)." [Online].
Available: https://serc.carleton.edu/research_education/geochemsheets/techniques/XRD.html. [Accessed: 18-Apr-2018].

[54] "Four-point resistivity measurements." [Online]. Available: http://lamp.tu-graz.ac.at/~hadley/sem/4pt/4pt.php. [Accessed: 28-Apr-2018].

[55] [Online]. Available: http://marriott.tistory.com/97. [Accessed: 20-Apr-2018].

[56] "Characterization and hydrogen gas sensing properties of TiO2 thin films prepared by sol–gel method." [Online].
Available: https://www.researchgate.net/publication/232956893_Characterization_and_hydrogen_gas_sensing_properties_of_TiO2_thin_films_prepared_by_sol-gel_method.
[Accessed: 28-Apr-2018].